Chapter 2

Deficiency in hematopoietic phosphatase Ptpn6/Shp1 hyperactivates the innate immune system and impairs control of bacterial infections in zebrafish embryos

Zakia Kanwal, Anna Zakrzewska, Jeroen den Hertog, Herman P. Spaink, Marcel J.M. Schaaf, and Annemarie H. Meijer

Abstract

Deficiency in the protein-tyrosine phosphatase SHP1/PTPN6 is linked with chronic inflammatory diseases and hematological malignancies in humans. Here we exploited the embryonic and larval stages of zebrafish (*Danio rerio*) as an animal model to study *ptpn6* function in the sole context of innate immunity. We show that *ptpn6* knockdown induces a spontaneous inflammation-associated phenotype at the late larval stage. Surprisingly, glucocorticoid treatment did not suppress inflammation under *ptpn6* knockdown conditions but further enhanced leukocyte infiltration and pro-inflammatory gene expression. Experiments in a germ-free environment showed that the late larval phenotype was microbe independent. When *ptpn6* knockdown embryos were challenged with *Salmonella typhimurium* or *Mycobacterium marinum* at earlier stages of development, the innate immune system was hyperactivated to a contra-productive level that impaired the control of these pathogenic bacteria. Transcriptome analysis demonstrated that KEGG pathways related to pathogen recognition and cytokine signaling were significantly enriched under these conditions, indicating that *ptpn6* functions as a negative regulator that imposes a tight control over the level of innate immune response activation during infection. In contrast to the hyperinduction of pro-inflammatory cytokine genes under *ptpn6* knockdown conditions, anti-inflammatory *il10* expression was not hyperinduced. These results demonstrate that *ptpn6* has a crucial regulatory function in preventing host-detrimental effects of inflammation and is essential for a successful defense mechanism against invading microbes.

Introduction

The innate immune system has been conserved in evolution from invertebrate to vertebrate organisms and plays an indispensable role in host protection against infections. The vertebrate innate immune system has been demonstrated to not only function as the first line of defense against microorganisms, but also to be required for activating the secondary adaptive defenses. However, if the innate immune system goes unchecked, the production of inflammatory mediators can cause considerable tissue damage. Recent studies indicate that defects in the initial sensing of microorganisms and allergens by the innate immune system can contribute to autoimmune and autoinflammatory diseases, which were classically viewed as specific disorders of the adaptive immune system (Beutler, 2009; Drexler and Foxwell, 2010; Theofilopoulos et al., 2011). In healthy individuals the innate immune response is tightly controlled by complex regulatory mechanisms that prevent excessive and chronic inflammation (O'Neill, 2008). The SHP1 phosphatase, encoded by the *PTPN6* gene, has been recognized as a critical factor in this process of negative regulation.

SHP1 belongs to the family of protein-tyrosine phosphatases (PTPs), which dephosphorylate phosphotyrosyl residues in proteins that are phosphorylated by protein-tyrosine kinases (PTKs). PTPs and PTKs function in a variety of cellular

processes, from cell survival to proliferation, differentiation, migration and immune responses. SHP1 (PTPN6) and SHP2 (PTPN11) are closely related non-receptor type PTPs, each having two Src homology 2 (SH2) domains amino-terminal to the phosphatase catalytic domain (Zhang et al., 2000; Tsui et al., 2006; Pao et al, 2007). While SHP2 is expressed ubiquitously, SHP1 is predominantly expressed in hematopoietic cell lineages, and it has been implicated in the regulation of a diverse range of cytokine receptors, growth factor receptors, and immunoreceptors. SHP1 has been shown to associate with immunoreceptor tyrosine-based inhibition motifs (ITIMs) in these receptors (Zhang et al., 2000; Tsui et al., 2006), and has been proposed to bind to ITIM-like motifs in various kinases, including IRAK1, ERK1/2, p38, JNK, JAK2, JAK3, TAK1, IKKα, and LYN (Abu-Dayyeh et al., 2008; Abu-Dayyeh et al., 2010).

SHP1 has been extensively studied after the discovery of two naturally occurring mutant mouse strains: motheaten (*me*), considered to carry a null allele of the *Ptpn6* gene, and motheaten viable (*mev*), which encodes a phosphatase with approximately 20% of wild type catalytic activity (Shultz et al., 1993; Tsui et al., 1993; Kozlowski et al., 1993). These mice suffer from severe immune disorders, with spontaneous inflammatory activity affecting multiple organs, including the lungs, kidney, joints, and skin, the latter resulting in their typical 'motheaten' appearance. The mutations result in lethal pneumonitis by three (*me*) or nine (*mev*) weeks of age. Backcrossing of *mev* mice to *rag1* null mutants (that do not contain mature T and B cells) did not alleviate the *motheaten* inflammatory disease, indicating that the function of myeloid cells rather than the function of the adaptive immune system is required for major aspects of the *shp1* mutant phenotype (Yu et al., 1996). Furthermore, pulmonary inflammation in *mev* mutants was found to depend strongly on the function of mast cells (Zhang et al., 2010). A viable hypomorphic allele of *Ptpn6, spin* (spontaneous inflammation), carrying a point mutation in one of the SH2 domains, was later described that elicits chronic inflammatory and autoimmune disease (Croker et al., 2008). Inflammation in *spin* mutants was triggered by the presence of microbes and found dependent on production of IL-1, subsequent IL-1 signaling, and the presence of neutrophils (Croker et al., 2008; Croker et al., 2011). Consistent with these findings, SHP1 was shown to negatively regulate Toll-like receptor (TLR)-mediated production of pro-inflammatory cytokines by suppressing the activation of MAPKs and the transcription factor NF-κB (An et al., 2008).

SHP1 has been associated with several human inflammatory diseases. In patients with psoriatic inflammatory skin disease, deficient SHP1 expression in T-cells has been observed (Eriksen et al., 2010). Furthermore, macrophages of multiple sclerosis (MS) patients display SHP1 deficiency concomitant with enhanced expression of genes mediating inflammatory demyelination in MS pathogenesis (Christophi et al., 2009). Finally, it has been suggested that altered expression of SHP1 may also be associated with human allergies and asthmatic disease, based on recent studies in mice that indicate a role of SHP1 in mast cells and allergic inflammatory responses (Zhu et al., 2010). In addition, SHP1 is considered a putative tumor suppressor. Decreased expression of SHP1 has been observed in many types of human lymphomas and

leukemias. The reduced levels of SHP1 in these malignancies have been attributed to mutations, epigenetic regulation, and post-transcriptional mechanisms (Wu et al., 2003; Witkiewicz et al., 2007). SHP1 has also been implicated as a negative regulator of insulin signaling and clearance of insulin in the liver, and has been linked to progression of diabetic retinopathy (Dubois et al., 2006; Geraldes et al., 2009).

As many recent studies have shown, the zebrafish embryo model has specific advantages not only for developmental biology but also for studying immunity, inflammation and infections (Lieschke and Trede, 2009; Martin and Renshaw, 2009; Meijer and Spaink, 2011). The embryo model is particularly useful for studying responses of the innate immune system, as macrophages and neutrophils develop during the first two days of embryogenesis, when the adaptive immune system is not yet in place (Lam et al., 2004). The zebrafish genome encodes orthologs of the majority of human PTPs, including *shp1/ptpn6* and *shp2/ptpn11a* (van Eekelen et al., 2010). We have previously shown that hematopoietic expression of *shp1/ptpn6* is conserved in zebrafish embryos and controlled by the transcription factor Pu.1 (Spi1), like its human counterpart (Zakrzewska et al., 2010; Wlodarski et al., 2007). The zebrafish embryo model was also exploited to study the role of *shp2* in early development and to investigate the cell biological effects of activating and inactivating mutations in Shp2 protein that underlie the Noonan and LEOPARD syndromes in humans. Defective Shp2 signaling induced cell movement defects as early as gastrulation and zebrafish embryos expressing Noonan or LEOPARD Shp2 displayed craniofacial and cardiac defects, reminiscent of human symptoms (Jopling et al., 2007).

Here we used morpholino knockdown to study the effect of *ptpn6* deficiency in zebrafish embryos. No visible phenotypic effects of *ptpn6* knockdown were observed during early development, but morphant larvae developed a late phenotype at 5 to 6 days post fertilization (dpf). Skin lesions in these morphants were reminiscent of phenotypes of the murine *ptpn6* mutants, *motheaten* and *spin*, which suffer from severe inflammation leading to patches of hair loss and foot lesions, as discussed above (Tsui et al., 1993; Croker et al., 2008). Based on leukocyte infiltration and pro-inflammatory gene expression we concluded that also the zebrafish *ptpn6* morphant phenotype is associated with an inflammatory response. We describe infection experiments of *ptpn6* morphants with bacterial pathogens at 1 dpf, which is several days prior to the manifestation of the late inflammation-associated phenotype. We observed that *ptpn6* morphants responded to bacterial challenge with increased induction of pro-inflammatory genes compared to wild type embryos, yet their ability to control these infections was severely impaired, indicating that this is not a functional response. In conclusion, our data demonstrate the role of *ptpn6* as a negative regulator of the innate immune system, which is important for a functional innate immune response during bacterial infections.

Materials and methods

Zebrafish husbandry

Zebrafish were handled in compliance with the local animal welfare regulations and maintained according to standard protocols (zfin.org). Zebrafish lines used in this study included AB/TL, *Tg(mpx:gfp)i114* (Renshaw et al., 2006), *Tg(fli1:EGFP)* (Lawson and Weinstein, 2002) and *Tg(-1.0pomca:GFP)zf44;Tg(prl:RFP)zf113* (Liu et al., 2006). Embryos were grown at 28.5–30°C in egg water (60 µg/ml Instant Ocean sea salts). For the duration of bacterial injections embryos were kept under anesthesia in egg water containing 200 µg/mL tricaine (Sigma-Aldrich). Embryos used for whole mount in situ hybridization and immunostaining were kept in egg water containing 0.003% 1-phenyl-2-thiourea (Sigma-Aldrich) to prevent melanization.

Morpholino knockdown

Morpholino oligonucleotides (Gene Tools) were diluted to the desired concentration in 1× Danieau buffer (58 mM NaCl, 0.7 mM KCl, 0.4 mM $MgSO_4$, 0.6 mM $Ca(NO_3)_2$, 5.0 mM HEPES; pH 7.6) containing 1% phenol red (Sigma-Aldrich) and approximately 1 nL was injected at the 1-2 cell stage using a Femtojet injector (Eppendorf). For knockdown of *ptpn6* two morpholinos were used, one targeting the exon 11/intron 11-12 splice junction (MO1: 5'ACTCATTCCTTACCCGATGCGGAGC3'; 0.0625 mM), and one targeting the translation start site (MO2: 5'CTGTGAAACCACCGAACCATCTTCC3'; 0.20 mM). As a control we used the standard control (SC) morpholino from GeneTools at the same concentrations as the *ptpn6* MOs.

Whole-mount in situ hybridization, immunodetection, TUNEL assay, and myeloperoxidase activity assay

For all assays embryos were fixed in 4% paraformaldehyde (PFA) in phosphate-buffered saline (PBS). Whole-mount in situ hybridization (WISH) using alkaline phosphatase detection with BM Purple substrate (Roche Diagnostics) was carried out as previously described (Stockhammer et al., 2009). Digoxigenin-labeled *mfap4* and *mpx* probes were generated as described in (Zakrzewska et al., 2010). Immunofluorescence stainings were performed with 1:500 dilutions of polyclonal rabbit Ab against phospho-Histone H3 (Santa Cruz) and L-plastin (Mathias et al., 2007). For detection, Alexa Fluor 568/488 goat anti-rabbit IgG secondary Ab (Molecular Probes) as described in (Cui et al., 2011) were used. DNA fragmentation during apoptotic cell death was examined by TUNEL using the ApopTag Peroxidase In Situ Apoptosis Detection Kit (Millipore) according to the manufacturer's instructions. Embryos were fixed, permeabilized, treated with Proteinase K and refixed in 4% PFA as for WISH. Embryos were then fixed in ethanol:acetic acid 2:1 for 15 min at -20ºC followed by PBS washes. After 15 min incubation in the equilibration buffer embryos were transferred to working strength TdT enzyme solution supplemented with 0.3% TritonX-100, and incubated for 1 h on ice followed by 1 h at 37ºC. The reaction was stopped by a 5 min wash in stop solution at room temperature, followed by 45 min

incubation at 37ºC and PBS washes. Subsequent immunodetection with alkaline phosphatase-conjugated anti-DIG Fab fragments and BM purple staining was performed as for WISH. Histochemical staining for Mpx activity was performed with the Peroxidase Leukocyte Kit (Sigma-Aldrich) as described in (Cui et al., 2011).

RNA isolation, quantitative RT-PCR, and RT-MLPA

RNA isolation and quantitative RT-PCR (qPCR) analysis was performed as described in (Stockhammer et al., 2009). Primer sequences for *ppial*, *il1b*, *mmp9*, *lgals*, *mpeg1*, *cxcr3.2*, *mfap4*, and *marco* are described in (Zakrzewska et al., 2010; Stockhammer et al., 2009). Additional primer sequences used were:
lyz: FW5'TGTCCTCGTGTGAAAGCAAGAC3', REV5'AGAATCCCTCAAATCCATCAAGCC3';
mpx: FW5'AAGACAATGCACGAGAGC3', REV5'GCAATGAAGCAAGGAACC3';
csf1r: FW 5'CTGCTGGTCGTAGAGGAG3', REV 5'TGTGAAGTCAGAGGAGG3';
ncf1: FW5'CACAGGATGGCTGAAACATACG3, REV5'TAGTGCTGGCTGGGAAAGAATC3'.
Reverse transcription – multiplex ligation-dependent probe amplification (RT-MLPA) was performed as described in (Rotman et al., 2011).

Germ-free experiments

For generating germ-free embryos we used a natural breeding method described in (Pham et al., 2008). Eggs were washed 3× in antibiotic gnotobiotic zebrafish medium (GZM) prior to performing morpholino injections in a down-flow cabinet using sterilized needles and equipment. Following injections, eggs were immediately washed with antibiotic GZM and were successively treated with PVP-I and bleach solutions. Embryos were grown in 6 well plates at 28°C wrapped in aluminum foil and sterile antibiotic GZM was refreshed daily. At the end of the experiment sterility was tested by plating media from the germ-free and conventionally raised embryos on tryptic soy agar plates.

Chemical treatments

Betamethasone 17-valerate (1 μM) , beclomethasone (25 μM), and prednisolone (25 μM) were dissolved in 0.1% DMSO and added directly to egg water at 1 dpf or 3 dpf, solutions were refreshed daily. Controls were treated with DMSO only. $CuSO_4$-induced inflammation was performed as in (d'Alencon et al., 2010).

Infection experiments

Salmonella typhimurium infections were performed using the *S. typhimurium* strain SL1027 and its isogenic LPS Ra mutant derivative SF1592, carrying the DsRed expression vector, pGMDs3 (van der Sar et al., 2003). For *Mycobacterium marinum* infection experiments the Mma20 strain was used expressing mCherry in pSMT3 vector (van der Sar et al., 2004). Bacteria were grown and prepared for injections as described in (Cui et al., 2011), and microinjected into the caudal vein of embryos at 28 hours post fertilization (hpf), using a dose of 200-250 CFUs of *S. typhimurium* or 100 CFU of *M.*

marinum per embryo. After injections embryos were transferred to fresh egg water and incubated at 28°C. For plating assays, infected embryos were homogenized using a Retsch mixer mill with a metal bead for 1 min at maximum speed.

Microarray analysis

For microarray analysis of *S. typhimurium* infection in *ptpn6* morphants, three independent infection experiments were performed. In each experiment, RNA was isolated from pools of 15-20 embryos per treatment group. Knockdown of *ptpn6* was performed using MO1 and control embryos were injected with Danieau buffer/phenol red. The *ptpn6* morphants and control embryos were infected at 28 hpf with *S. typhimurium* SL1027 bacteria, or mock-injected with PBS as a control. RNA extraction was performed at 8 hpi. Microarray analysis was performed using a previously described custom-designed 44K Agilent chip (Agilent Technologies) (Stockhammer et al., 2009). All RNA samples were labeled with Cy5 and hybridized against a Cy3-labeled common reference, which consisted of a mixture of all samples from the infection study. Labeling, hybridization and data analysis using Rosetta Resolver 7.0 was performed as previously described (Stockhammer et al., 2009). The raw data were submitted to the Gene Expression Omnibus database under accession no. GSE34930. KEGG pathway analysis was performed using DAVID v6.7 (http://david.abcc.ncifcrf.gov/home.jsp) (Huang da et al., 2009).

Microscopy and image analysis

Bright field images of embryos were obtained with a Leica M165C stereomicroscope equipped with a DFC420C digital color camera (Fig. 1; Fig. 2 A-D; Fig. 3 E-H; Supplementary Fig. S1 C, D) Composite images of different focal planes were created with Adobe Photoshop. Fluorescence images were taken with a Leica MZ16FA stereo fluorescence microscope equipped with a DFC420C digital color camera (Fig. 2 E-L ; Fig. 3 A, B, I-L; Fig. 5 C-F, H-M; Supplementary Fig. S1 E-H, K, L;). Overlay images of bright field and fluorescence stereomicroscopy were made in Adobe Photoshop. Confocal microscopy was performed with a Leica TCS SPE confocal microscope (Fig. 3 C, D: HC PLAN APO objective 20x/0.70 NA; Fig. 4 I-T: HCX APO objective 40x/0.80 NA; Fig. 5 N-Q) or Zeiss LSM5 Exciter system (Fig. 4 A-F: APO objective 10x/0.3 N/A). Maximum intensity projections of z-stacks of different focal planes were obtained using image J. Pixel counts on stereo fluorescence images were performed as described in (Stoop et al., 2011).

Results

Knockdown of *ptpn6* causes a late phenotype in zebrafish larvae that is characterized by enhanced proliferation, apoptosis, and inflammation

In order to study the function of the *ptpn6* gene in zebrafish, a knockdown study of this gene was performed using a splice blocking morpholino that causes deletion of the phosphatase catalytic domain (MO1) and a translation blocking morpholino (MO2) (Supplementary Fig. S1 A, B). Both morpholinos did not have strong effects on embryo morphology at 1-3 dpf, except that the heads and eyes of *ptpn6* morphants were slightly smaller compared with the controls (Fig. 1 A, B, H, I; Fig. 2). Furthermore, L-plastin immunostaining, *in situ* hybridization with *mfap4* and *mpx* markers, and Mpx activity assays demonstrated that macrophage and neutrophil numbers and the migratory responses of these cells towards injury were normal (Fig. 2).

However, at later stages of development, pleiotropic effects on larval morphology were observed that became progressively severe. At 3 dpf, some embryos showed a minor oedema of the heart cavity (Fig. 1 B, I), which became more prominent at 4 dpf (Fig. 1 C, J). At 5-6 dpf, morphant larvae additionally developed lesions on the eyes and skin, and in severe cases they also developed oedema between the trunk and the yolk sac and yolk extension (Fig. 1 D-G, K-N). After injection with MO1 between 80-90% of the larvae at 5-6 dpf showed these phenotypic abnormalities, while the effect of MO2 injection was lower, with only 5-10% of larvae displaying severe oedema and skin lesions (Supplementary Fig. S1 C, D). The heart beat frequency was unaffected in *ptpn6* morphants until 4 dpf, but was approximately 40% reduced in larvae of 6 dpf, as the likely result of the increased cardiac oedema at this stage (data not shown). Morpholino injection of *Tg(fli1:EGFP)* embryos did not reveal defects in vascular development (Supplementary Fig. S1 E-H).

Since mammalian *ptpn6*/*shp1* has been implicated in negative regulation of growth factor, MAPK, and NF-κB signaling pathways, we investigated proliferation, apoptosis, and inflammation in *ptpn6* morphants. Phosphohistone H3 immunolabeling revealed increased numbers of mitotic cells in *ptpn6* morphants in a specific region on the dorsal side of the brain and in the retina at 5 dpf (Fig. 3 A-D). Furthermore, increased numbers of apoptotic cells were detected with a TUNEL assay, particularly in the brain and in the region of cardiac oedema at this stage (Fig. 3 E-H). To determine if the phenotype of the zebrafish *ptpn6* morphants was associated with inflammation, we performed immunofluorescence staining using anti-L-plastin Ab, which stains all leukocytes (Mathias et al., 2007). The results showed that leukocytes in 5 dpf *ptpn6* morphants accumulated around the oedemic area of the heart cavity and at skin lesions, while they had largely disappeared from their normal location in the caudal hematopoietic tissue (Fig. 3 I-L). In addition, we checked the expression of the pro-inflammatory genes *il1b* and *mmp9*. Quantitative RT-PCR (qPCR) showed that, concomitant with the appearance of the strong phenotypic defects at 5-6 dpf, the

expression levels of *il1b* and *mmp9* were enhanced in *ptpn6* MO1 and MO2 morphant embryos compared to the controls at 5dpf and 6dpf, but not at 4dpf (Fig. 3 M-P). We conclude, based on leukocyte infiltration and enhanced *il1b* and *mmp9* expression, that the late pleiotropic phenotype of *ptpn6* morphant larvae is associated with inflammation.

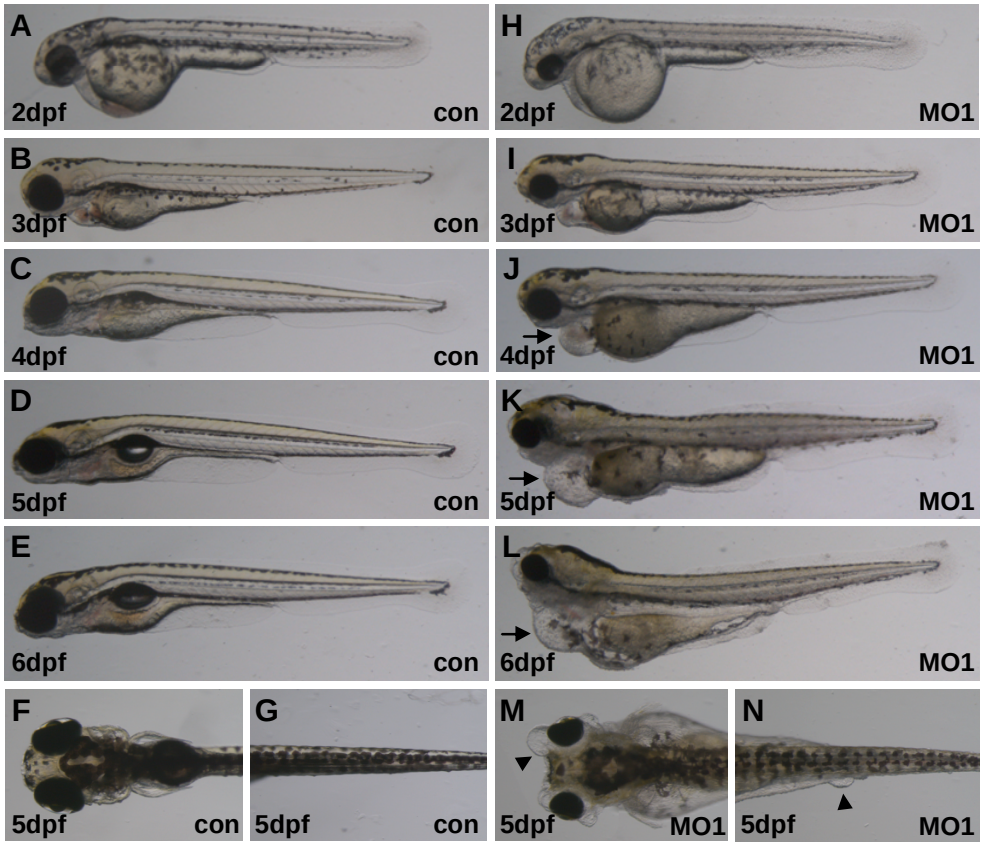

Figure 1. Late pleiotropic phenotype in *ptpn6* morphant zebrafish larvae. (A-G) Embryos injected with standard control morpholino (con). (H-N) embryos injected with *ptpn6* morpholino (MO1). Phenotypes are shown at 2-6 dpf in lateral (A-E, H-L) or dorsal view (F, G, M, N) with the anterior side to the left. Dorsal views show head and trunk (F, M) or the tail region (G, N). Skin lesions in *ptpn6* morphants are indicated with arrow heads and cardiac oedema is indicated with arrows.

The *ptpn6* morphant phenotype is independent of the presence of microbes

Since inflammation might be triggered by the presence of microbes, we investigated whether the zebrafish *ptpn6* morphant phenotype also developed in a germ-free environment. To this end, eggs were bleached, treated with iodine, and cultured in the presence of antibiotic and antifungal compounds following established protocols (Pham et al., 2008). At the end of the experiment sterility was confirmed by plating culture medium on tryptic soy agar plates, showing that bacterial colonies developed from

conventionally reared larvae but not from germ-free cultured larvae**.** When reared in the germ-free environment, 80-90% of the *ptpn6* morphant larvae developed oedema and skin lesions, similar to the conventionally raised morphant larvae. Therefore, the inflammation-associated phenotype of *ptpn6* morphants is apparently not driven by the presence of culturable microbes.

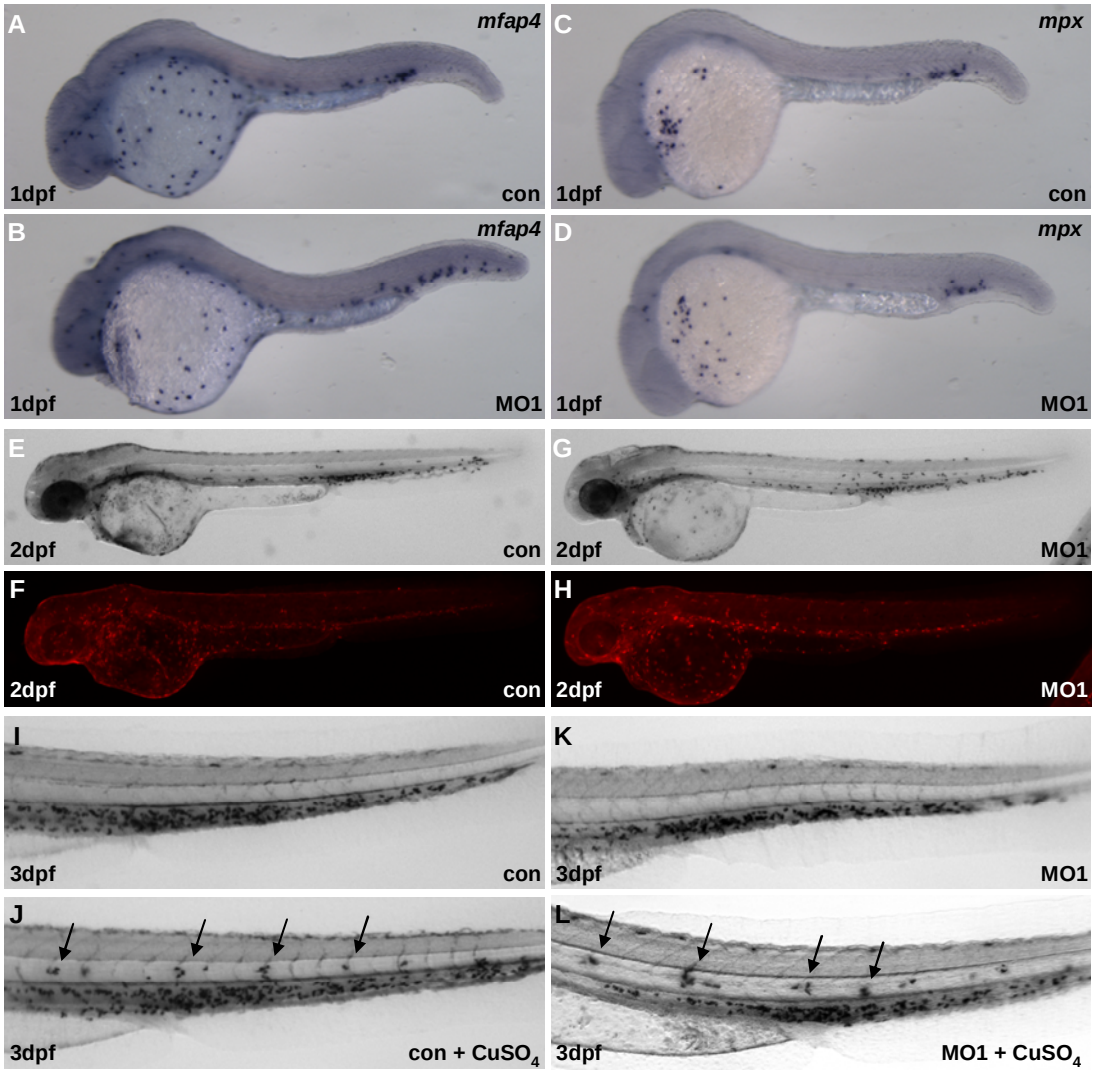

Figure 2. Unaltered leukocyte development and migratory response in *ptpn6* morphants. (A, B) In situ hybridization with macrophage marker *mfap4* (Zakrzewska et al., 2010) at 1 dpf. (C, D) In situ hybridization with neutrophil marker *mpx* at 1 dpf. (E, G) Histochemical staining for Mpx enzyme activity at 2-3 dpf. (F, H) immunolabeling of the same embryos as in E and G with Ab against the general leukocyte marker L-plastin. (I-L) Histochemical staining for Mpx enzyme activity in larvae incubated for 2 h with (J, L) or without (I, K) 10 µM CuSO4 at 3 dpf. Chemically induced inflammation by CuSO4 treatment (d'Alençon *et al* 2010) is due to damage of hair cells of the lateral line neuromasts, which attracts neutrophils (arrows in J, L). Embryos were injected with standard control (con) or *ptpn6* morpholino (MO1) and are shown in lateral view with the anterior to the left. The images are representative examples of ≥ 20 larvae in each group.

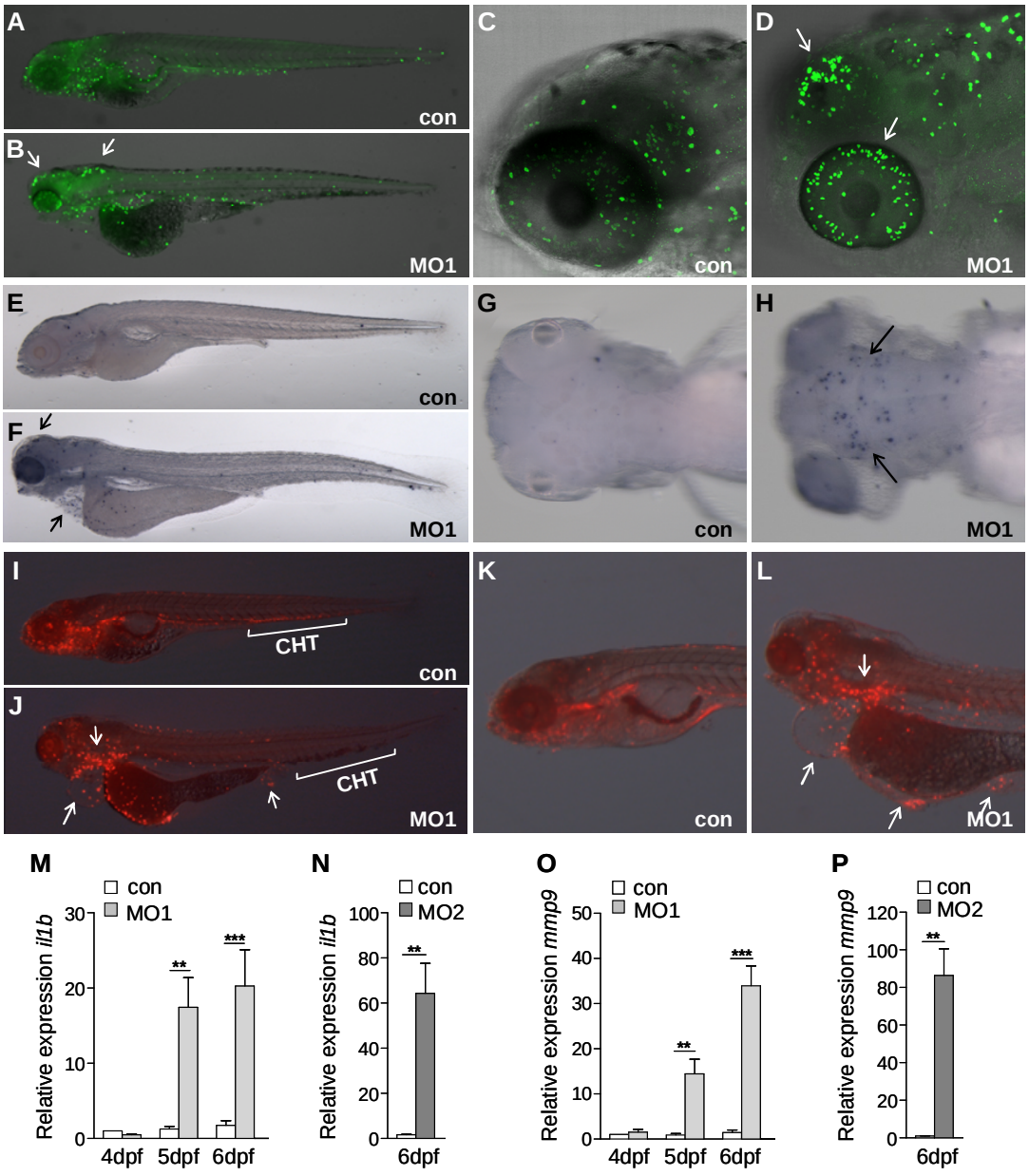

Figure 3. Enhanced proliferation, apoptosis, and inflammation in *ptpn6* morphants. (A-D) Phosphohistone H3 immunolabeling (E-H) TUNEL assay. (I-L) Immunolabeling with Ab against the general leukocyte marker L-plastin. Embryos were injected with standard control (con) or *ptpn6* morpholino (MO1) and all assays were performed at 5 dpf. Larvae or head details are shown in lateral (A- D, E, F, I-L) or dorsal (G, H) view with the anterior to the left. Stereo microscope images (A, B, E-L) and confocal Z-stack projections (C, D, transmitted light and fluorescence overlay) are representative examples of ≥ 20 larvae in each group. Arrows indicate regions with increased numbers of proliferating cells (B, D), increased numbers of apoptotic cells (F, H), and accumulation of leukocytes around sites of cardiac oedema and skin lesions (J, L) in *ptpn6* morphants. Also note the absence of immune cells in the caudal haematopoietic tissue (CHT) of *ptpn6* morphants (J) compared with the control (I). (M-P) Increased expression of proinflammatory genes in *ptpn6* morphants. Embryos were injected with splice blocking (MO1) or translation blocking (MO2) morpholinos targeting *ptpn6* or with standard control

morpholino (con). RNA was isolated at 4-6 dpf from pools of 10-20 larvae, which were picked randomly in the case of con and MO1 morpholino injections. In the case of MO2, which has a lower penetrance, 10-20 larvae showing the oedema and skin lesion phenotype were selected. Gene expression levels of *il1b* (M, N) and *mmp9* (O,P) were determined by qPCR and relative expression levels are shown with the lowest expression level set at 1. Data are the mean ± SEM of three independent experiments. Asterisks indicate significant differences (**, $P < 0.01$; ***, $P < 0.001$) tested with an unpaired t-test.

Glucocorticoid treatment enhances the *ptpn6* morphant phenotype

The immunosuppressive action of glucocorticoids is known to be conserved between zebrafish and mammals (Schaaf et al., 2009). Since the *ptpn6* morphant phenotype was associated with enhanced pro-inflammatory gene expression and leukocyte infiltration of affected tissues, we tested whether these effects could be suppressed by glucocorticoid treatment. Surprisingly, treatment with the synthetic glucocorticoid betamethasone 17-valerate, which was previously demonstrated to act as a potent glucocorticoid in zebrafish (Schoonheim et al., 2010), enhanced rather than suppressed the development of oedema and skin lesions in *ptpn6* morphants. Treatment with two other glucocorticoids, beclomethasone and prednisolone, also enhanced the development of oedema and skin lesions (data not shown). The affected tissues in morphants treated with betamethasone 17-valerate were accompanied by a more abundant leukocyte infiltration, as demonstrated using a transgenic marker line for neutrophils (*Tg(mpx:gfp)i114,* (Renshaw et al., 2006) and by L-plastin-immunostaining of neutrophils and macrophages (Fig. 4 A-F). In addition, approximately 10% of *ptpn6* morphants that were treated with betamethasone 17-valerate from 1 dpf died at 5 dpf, while all untreated morphants were viable until 7-8 dpf. In line with the enhanced phenotype, the induction levels of *il1b* and *mmp9* were also further increased in morphants treated with betamethasone 17-valerate as compared to the control group (Fig. 4 G, H). The increase of *il1b* and *mmp9* at 5 dpf was more pronounced when betamethasone 17-valerate treatment was performed for 4 days starting at 1 dpf compared to a 2-day treatment starting at 3 dpf (Fig. 4 G, H). However, no general insensitivity to glucocorticoids was observed. Expression of *fkbp5*, a well-known glucocorticoid receptor target gene (Schaaf et al., 2009), was inducible by betamethasone 17-valerate in both *ptpn6* morphants and control embryos (data not shown). In addition, betamethasone 17-valerate could still repress the expression of the *pomc* gene in the anterior lobe of the pituitary gland of *ptpn6* morphants (Fig. 4 I-T), a phenotype often used to score for glucocorticoid responsiveness (Schoonheim et al., 2010). Overall, these results show that glucocorticoids are not able to suppress the inflammatory response observed in *ptpn6* morphants, and that instead they unexpectedly enhance this response.

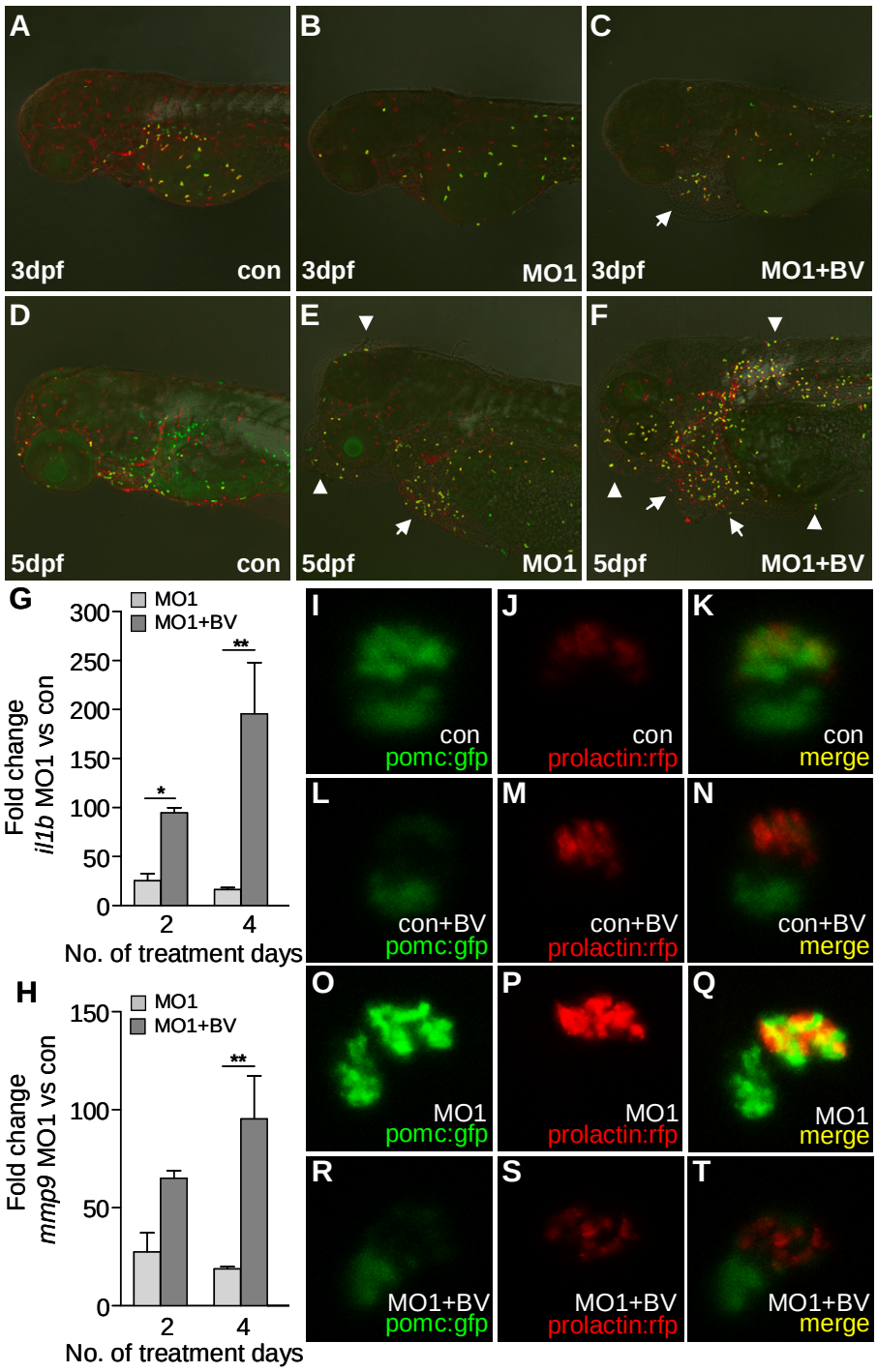

Figure 4. Enhanced leukocyte infiltration and inflammatory gene expression by glucocorticoid treatment of *ptpn6* morphants. (A-F) Embryos of the *Tg(mpx:gfp)i114* neutrophil marker line were injected with standard control (con) or *ptpn6* morpholino (MO1) and treated at 1 dpf with 1 µM betamethasone 17-valerate (BV) in 0.1% DMSO or with 0.1% DMSO alone as a control. Immunolabelling with Ab against the general leukocyte marker L-plastin was performed at 3 and 5 dpf. Confocal Z-stacks (fluorescence and transmission overlay) of the larval heads (lateral view, anterior to the left) are representative examples of ≥

20 larvae in each group. Accumulation of leukocytes around sites of cardiac oedema and skin lesions in *ptpn6* morphants is indicated with arrows and arrowheads, respectively. (G,H) Embryos were injected with standard control or *ptpn6* (MO1) morpholino and treated with betamethasone 17-valerate (BV) for 2 days starting at 3 dpf or for 4 days starting at 1 dpf. RNA was isolated at 5 dpf from pools of 10-20 larvae. Gene expression levels of *il1b* (G) and *mmp9* (H) were determined by qPCR and are represented as the fold increase of expression level of the MO1 group relative to that of the control morpholino group. Data are the mean ± SEM of three independent experiments. Asterisks indicate significant differences (* , $P < 0.05$; **, $P < 0.01$) tested by two-way ANOVA analysis with Bonferroni method as post-hoc test. (I-T) Glucocorticoid repression of *pomc* expression in the anterior lobe of the pituitary gland in *ptpn6* morphants and control embryos. Double transgenic zebrafish embryos expressing prolactin:rfp in the anterior lobe of the pituitary gland and pomc:gfp in the anterior and posterior lobes (*Tg(-1.0pomca:GFP)zf44;Tg(prl:RFP)zf113*, Liu et al., 2006) were injected with standard control (con, I-N) or *ptpn6* (MO1, O-T) morpholinos and treated from 1 dpf with 1 μM betamethasone 17-valerate (BV) in 0.1% DMSO (L-N, R-T) or with 0.1% DMSO as a control (I-K, O-Q). The pituitary gland was imaged at 5 dpf and confocal Z-stacks are representative of 15-20 embryos per group. In *ptpn6* morphants the pituitary gland is twisted to the right compared to that in control embryos, but pomc:gfp expression in the anterior lobe is down-regulated by glucocorticoid treatment similar as it is in the control embryos.

Knockdown of *ptpn6* impairs the ability of embryos to combat *S. typhimurium* and *M. marinum* infections

To investigate the function of *ptpn6* in the innate immune response to infection, we challenged *ptpn6* morphants and control embryos by intravenous injection of *S. typhimurium* bacteria. Importantly, bacterial injections were performed at 28 hpf, i.e. several days before the appearance of inflammation and other phenotypic effects in *ptpn6* morphants. In both *ptpn6* MO1 morphants and controls, *S. typhimurium* infection was lethal around 24-30 hours post infection (hpi). However, CFU counts at 2, 8 and 20 hpi showed that *S. typhimurium* proliferated faster in the *ptpn6* morphants (Fig. 5 A). Subsequently, we performed infections with the non-pathogenic *S. typhimurium* LPS O-Ag mutant strain Ra (van der Sar et al., 2003). While this Ra strain hardly proliferated in control embryos, clear proliferation of the DsRed-labeled Ra bacteria was observed in approximately 55% of *ptpn6* MO1 morphants at 1 day post infection (Fig. 5 B-D). At 5 days post infection (dpi), control embryos had cleared the infection or showed very low DsRed fluorescence signal, while the majority of *ptpn6* morphants were heavily infected or had died at 5 dpi (Fig. 5 B, E, F). Increased proliferation of wild type and Ra *S. typhimurium* bacteria was also observed in embryos injected with *ptpn6* MO2 (Supplementary Fig. S1 I-L).

Next we examined the response of *ptpn6* morphants to infection with *M. marinum*, a pathogen known to cause a chronic infection in zebrafish embryos, whereby infected and uninfected macrophages cluster into aggregates that resemble tuberculous granulomas (Davis et al., 2002; van der Sar et al., 2009). At 3 dpi *ptpn6* morphants showed increased fluorescence signal of mCherry labeled *M. marinum* bacteria and increased numbers of granuloma-like aggregates compared to control embryos (Fig. 5 G-I). At 4 and 5 dpi, granulomas in *ptpn6* morphants further increased in size compared

to those in control embryos (Fig. 5 G, J-M). Furthermore, immunohistochemical analysis using an L-plastin Ab of granulomas at 4 dpi showed that the bacteria were mostly extracellular in *ptpn6* morphants, while in control embryos bacteria were mostly contained within L-plastin-labeled leukocytes (Fig. 5 N-Q).

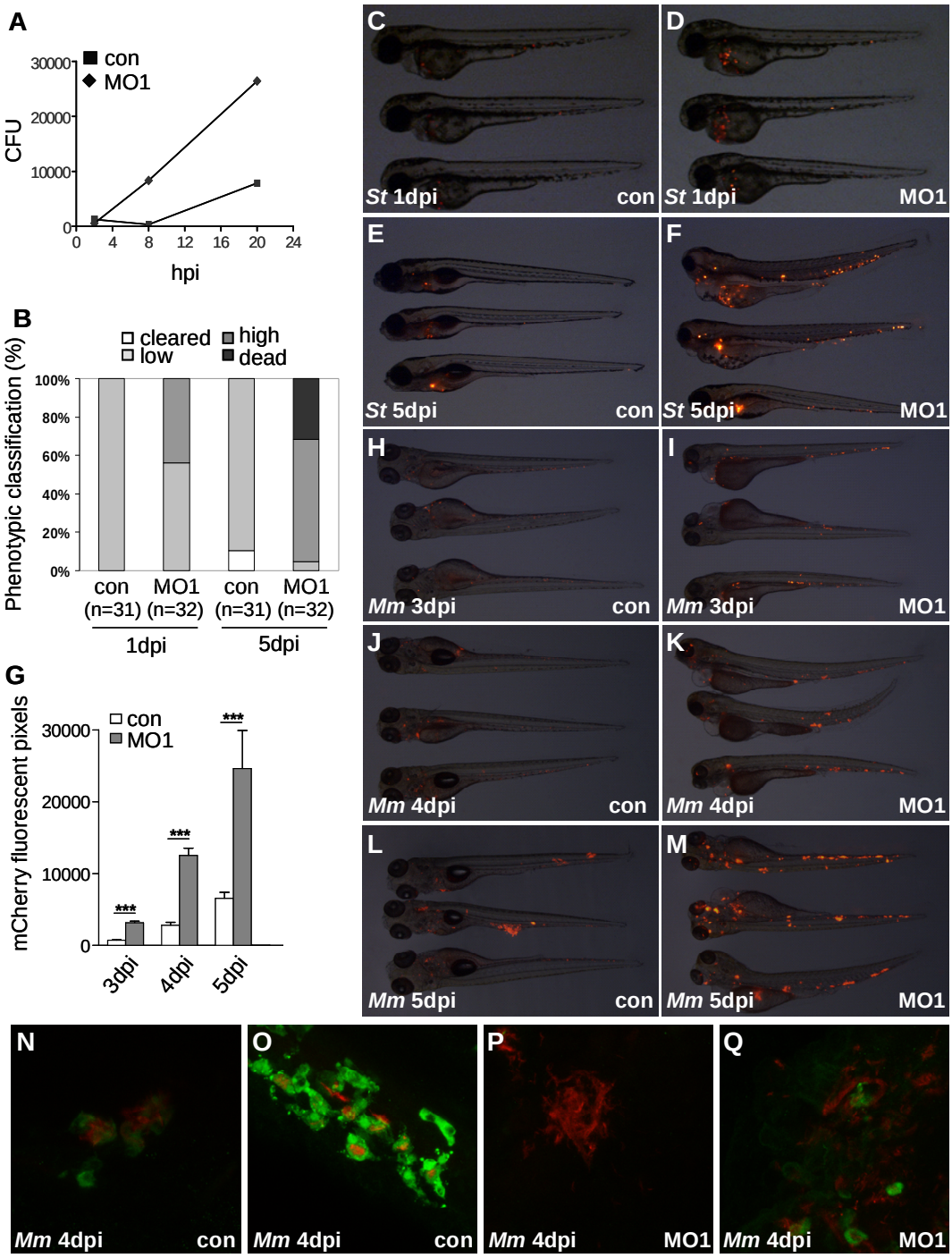

Figure 5. Impaired control of *S. typhimurium* and *M. marinum* infection in *ptpn6* morphants. (A) Infection with *S. typhimurium* wild type strain. Embryos were injected with

standard control morpholino (con) or *ptpn6* MO1 and infected with *S. typhimurium* at 28 hpf. Groups of 5 embryos were crushed in PBS at 2, 8, and 20 hpi, and dilutions were plated for CFU counting on LB medium with carbenicillin selection of the DsRED marker plasmid in *S. typhimurium*. A representative example of three independent experiments is shown. (B-F) Infection with *S. typhimurium* LPS O-Ag mutant Ra strain. Embryos were injected with standard control morpholino (con) or *ptpn6* MO1 and infected with *S. typhimurium* Ra at 28 hpf. The bacterial burden was analyzed at 1 and 5dpi based on fluorescence of the DsRED marker plasmid. A quantification of phenotypes (B) and stereo fluorescence images (lateral view, anterior to the left,) of 3 embryos per group (C-F) are shown for a representative example of three independent experiments. The bacterial burden in embryos at 1 dpi was scored as low (representative image in C) or high (representative image in D). At 5 dpi embryos had either cleared the infection, or had died, or showed low (representative image in E) or high (representative image in F) bacterial burden. (G-Q) Infection with *M. marinum* Mma20 strain. Embryos were infected with approximately 100 CFU at 28 hpf, and formation of *M. marinum* granulomas was analyzed at 3, 4 and 5 dpi based on fluorescence of the mCherry marker plasmid. Fluorescence images of more than 60 embryos per treatment group accumulated from two independent experiments were analyzed with pixel quantification software (Stoop et al., 2011) including an uninfected group as the blank. Pixel quantification data ± SEM (G) and representative fluorescence images (lateral view, anterior to the left) of 3 embryos per group (H-M) are shown. (N-Q) Confocal Z-stacks of granulomas in *ptpn6* MO1 morphants and control embryos.

In conclusion, when challenged with bacteria during early development, prior to the manifestation of the late inflammation-associated phenotype, *ptpn6* morphants were severely impaired in their ability to control the progression of infection. This impaired control was observed with *S. typhimurium* and *M. marinum* strains that induce very different pathologies, indicating a general inability of *ptpn6* morphants to mount a functional immune response.

Bacterial challenge of *ptpn6* morphants leads to hyperinduction of *il1b* and *mmp9* gene expression

To further investigate the function of *ptpn6* in the innate immune response to infection, we performed qPCR analysis for two genes, *il1b* and *mmp9*, which were previously shown to represent robust pro-inflammatory markers associated with bacterial infection (Stockhammer et al., 2009) and with the late phenotype observed after *ptpn6* knockdown (see above). We chose to analyze the response to *S. typhimurium* infection at 8 hpi (36 hpf) based on a previous time-course analysis (Stockhammer et al., 2009). As expected, control embryos showed a strong induction of *il1b* and *mmp9* expression levels. Upon knockdown of *ptpn6* with MO1 or MO2, the induction levels of *il1b* and *mmp9* were significantly higher than in the control embryos (Fig. 6 A, B). Therefore, we conclude that *ptpn6* functions as a negative regulator of *il1b* and *mmp9* induction during *S. typhimurium* infection. Unlike the strong pro-inflammatory gene expression that is induced by *S. typhimurium* infection at 8 hpi (Fig. 6 A, B), control embryos or *ptpn6* morphants infected with *M. marinum* did not show significant *il1b* and *mmp9* induction at this time point (Fig. 6 C, D). However, at 3 dpi *mmp9* (but not *il1b*) expression was increased in *M. marinum*-infected *ptpn6* morphants compared to

uninfected morphants and infected controls (Fig. 6 C, D). In summary, a hyperinduction of pro-inflammatory genes was observed upon bacterial infections of *ptpn6* morphants, yet their ability to control these infections was impaired.

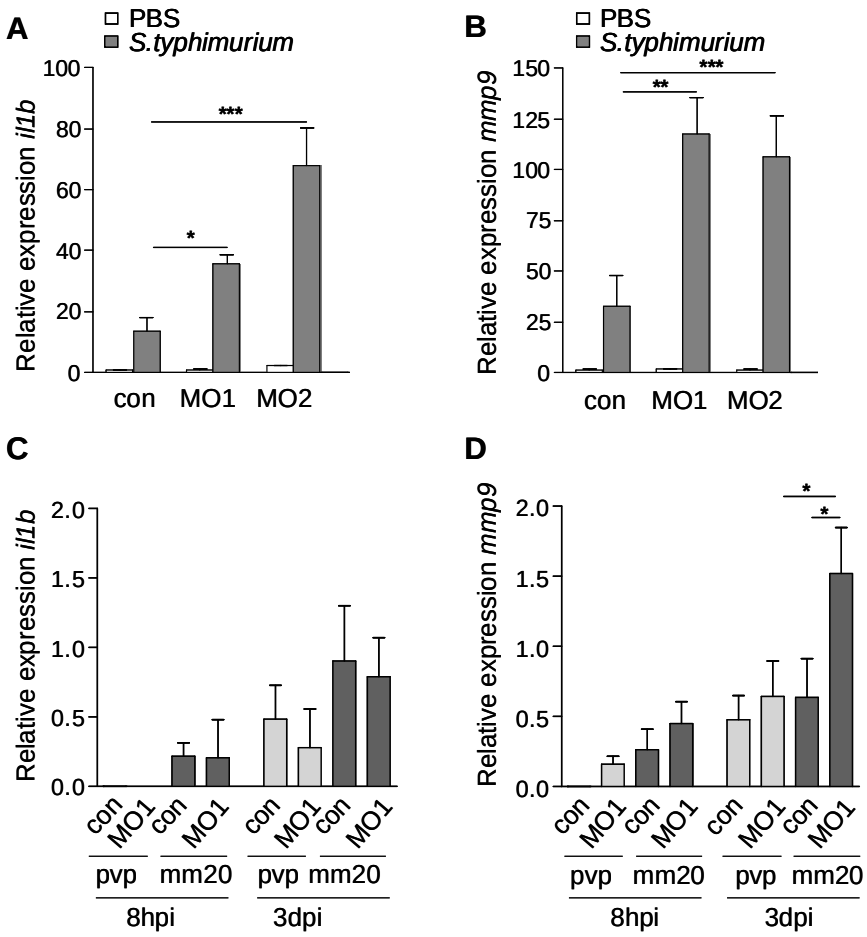

Figure 6. Increased induction of *il1b* and *mmp9* expression in *ptpn6* morphants challenged with bacterial pathogens. (A, B) qPCR analysis of *il1b* (A) and *mmp9* (B) expression in RNA samples of PBS-injected or *S. typhimurium*-infected control embryos (con) and *ptpn6* morphants (MO1 and MO2). Embryos were injected at the 1-2 cell stage with standard control (con) or *ptpn6* (MO1 or MO2) morpholinos, injected with PBS or with 250 CFU of *S. typhimurium* at 28 hpf, and RNA was isolated at 8 hpi for qPCR analysis. Relative expression levels are shown with the lowest expression level set at 1. Values are the means ± SEM of three biological replicates. (C, D) Gene expression levels of *il1b* (C) and *mmp9* (D) in response to *M. marinum* infection. Embryos were injected with standard control morpholino (con) or *ptpn6* MO1, approximately 100 CFU of *M. marinum* bacteria were injected at 28 hpf, and RNA was isolated at 8 hpi or 3 dpi. Relative expression levels are shown with the lowest expression level set at 1. Data are plotted on a logarithmic scale and are the mean ± SEM of three replicate experiments. Asterisks indicate significant differences (*, $P < 0.05$; **, $P < 0.01$; ***, $P < 0.001$) tested by two-way ANOVA analysis with Bonferroni method as post-hoc test.

Microarray analysis demonstrates an overall enhancement of the innate immune response to *S. typhimurium* infection upon *ptpn6* knockdown

The *S. typhimurium* infection model was chosen for further investigation of the specific effects of *ptpn6* knockdown on the innate immune response by microarray analysis. The advantage of this model for functional analysis of *ptpn6* was that the response to *S. typhimurium* infection can be analyzed at 36 hpf (8 hpi) (Stockhammer et al., 2009; Ordas et al., 2011), thus avoiding that the microarray analysis is affected by secondary effects of the late inflammatory phenotype (observed at 4-6 dpf). RNA samples from infected and mock-injected *ptpn6* MO1 morphants or control embryos from three replicate experiments were analyzed using a common reference approach (Fig. 7 A). First we analyzed the basal expression differences between mock-injected *ptpn6* morphants and control embryos. KEGG pathway analysis showed that p53 signaling and cell cycle were the most significantly affected pathways, and minor effects were observed on cytosolic DNA-sensing, sucrose metabolism and pyrimidine metabolism (Fig. 7 B). There was little overlap with the genes that were induced by infection in *ptpn6* morphants: only 7% of the microarray probes that showed basal expression differences between controls and *ptpn6* morphants were responsive to infection in *ptpn6* morphants (Fig. 7 B). The infection-responsive gene set showed significant alteration of many KEGG pathways related to the immune response, such as TLR, NLR, RIG-I, p53, MAPK, and JAK-STAT signaling (Fig. 7 B). For further analysis of *ptpn6* function we concentrated on the differences between the responses to infection in *ptpn6* morphants and controls.

The total number of probes showing significant responsiveness to infection was approximately 2-fold larger in *ptpn6* morphants than in controls (Fig. 7 C). Furthermore, the absolute fold changes of many infection-responsive probes were larger in *ptpn6* morphants (see Supplementary Table 1 for a complete overview of the microarray data). In fact, a total of 598 probes (representing 258 different genes) showed significantly higher up-regulation in *ptpn6* morphants and 78 probes (representing 51 different genes) showed significantly stronger down-regulation (Fig. 8). Analysis of the gene group with higher up-regulation in *ptpn6* morphants showed significant overrepresentation of TLR, NLR, RIG-I, p53, MAPK, JAK-STAT and other immune-related KEGG pathways (Fig. 7 C). More specifically, genes showing higher up-regulation in *ptpn6* morphants included cytokine/chemokine/interferon genes such as *il1b*, *il8*, *tnfa*, *tnfb*, and *ifnphi1*, matrix metalloproteinases such as *mmp9* and *mmp13*, and many transcriptional regulators of the ATF, CEBP, AP1, NFκB, and STAT families (Fig. 8). The higher up-regulation of *il1b* and *mmp9* was consistent with the qPCR experiments described above (Fig. 6 A, B) and with qPCR validation of the samples used for the microarray study (Supplementary Fig. S2 A, B). As observed in previous *S. typhimurium* infection studies, several negative regulators of immunity signaling are induced concomitantly with the induction of pro-inflammatory genes (Stockhammer et al., 2009; Ordas et al., 2011). Similar to the increased induction of pro-inflammatory

genes, infected *ptpn6* morphants also showed increased induction levels of several of these negative regulators, such as *irak3*, *socs3a* and *socs3b,* and NFκB inhibitor genes (*nfkbiaa*, *nfkbiab*, *nfkbib*, *nfkbiz*). In contrast, the anti-inflammatory cytokine gene *il10* (represented by 4 probes on the array) did not show increased induction in *ptpn6* morphants.

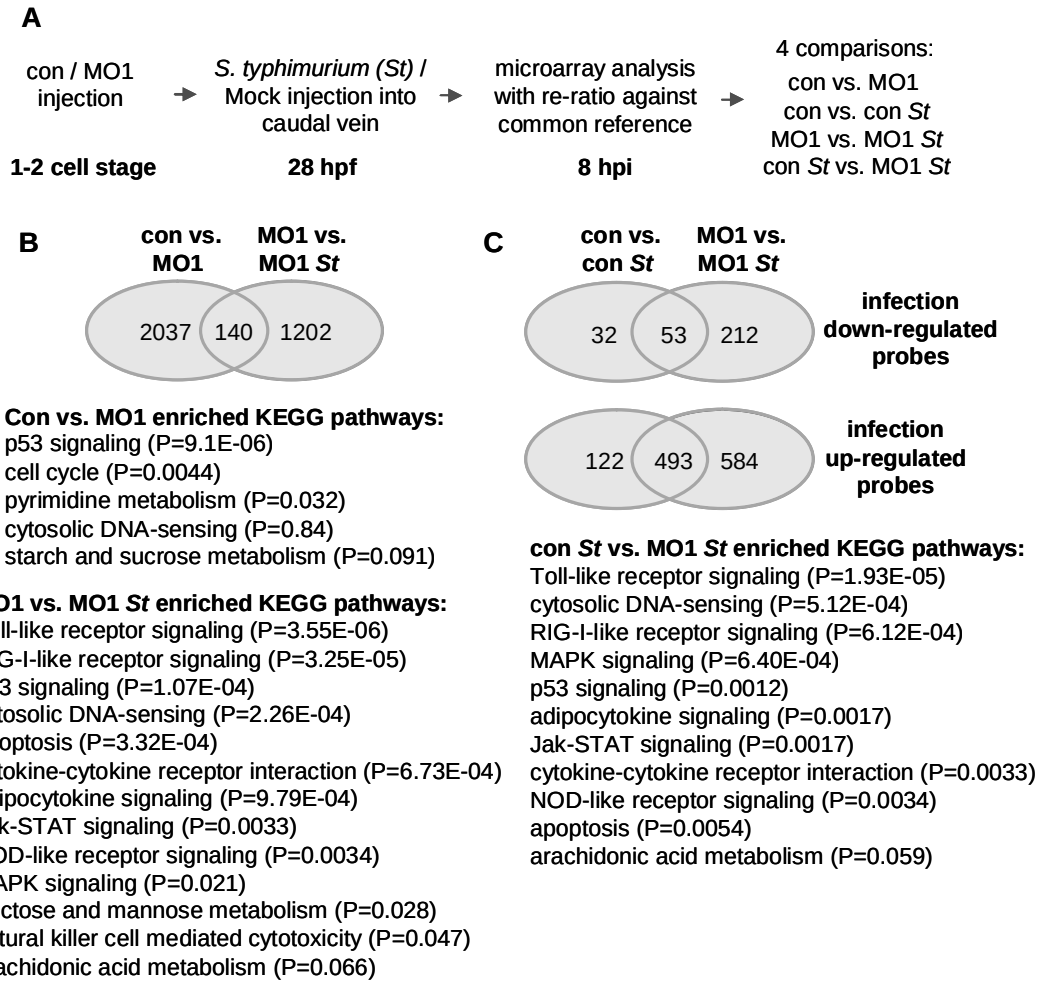

Figure 7. Enhanced innate immune response to *S. typhimurium* in *ptpn6* morphants. (A) Experimental set-up of the microarray analysis. Embryos were injected with *ptpn6* MO1 or Danieau's buffer at the 1-2 cell stage, and approximately 250 CFU of *S. typhimurium* bacteria were injected into the caudal vein at 28 hpf after the onset of the blood circulation, or PBS was injected as a control. Microarray analysis was performed on RNA samples extracted from pools of 15-20 embryos at 8 hpi. RNA samples from the four treatment groups (control/PBS, control/*S. typhimurium*, *ptpn6* MO1/PBS, *ptpn6* MO1/*S. typhimurium*) were obtained from three independent experiments and hybridized against a common reference consisting of RNA from all treatment groups. Next, four expression ratios were derived by Rosetta Resolver re-ratio analysis of the sample data against the common reference. The significance cut-offs were set an absolute fold change ≥1.5 and $P \leq 0.0001$. (B) Venn diagram showing the overlap between the effect of *ptpn6* knockdown on basal gene expression levels (con vs. MO1) and the effect of *S. typhimurium* on gene expression in *ptpn6* morphants (MO1 vs MO1 *St*). The numbers of probes

with significantly changed expression are shown in the Venn diagram and significantly enriched KEGG pathways for each comparison are indicated below. (C) Venn diagrams showing comparisons of the numbers of probes that were up-regulated or down-regulated by *S. typhimurium* infection in control embryos (con vs. con *St*) or in *ptpn6* morphants (MO1 vs. MO1 *St*). KEGG pathways that were significantly enriched in the dataset of infected *ptpn6* morphants compared with the dataset of infected controls (con *St* vs. MO1 *St*) are indicated below. A complete overview of the microarray data is given in Supplementary Table 1.

The smaller gene group that showed stronger down-regulation upon infection in *ptpn6* morphants than in the controls included two CCL chemokine genes (*ccl1* and *ccl-c11a*) and several leukocyte markers such as *coro1a*, *cpa5*, *cxcr3.2*, *lgals9l1*, *lcp1*, *lyz*, and *mpx* (Fig. 8). However, there was no generally enhanced down-regulation of leukocyte markers in infected *ptpn6* morphants, as *mpeg1* was less repressed in infected *ptpn6* morphants than in infected controls, and *csf1r* and *mfap4* showed unaltered expression under all conditions. qPCR analysis of leukocyte markers showed the same trend as the microarray data, particularly increased down-regulation of *lgals9l1*, *lyz*, and *mpx* during infection, less pronounced down-regulation of *mpeg1*, and unaltered expression of other markers, including *csf1r* and *mfap4* (Supplementary Fig. S2 C-F). In conclusion, microarray analysis indicated that under *ptpn6* knockdown conditions, embryos responded to *S. typhimurium* infection by an enhanced gene induction profile of the innate immune response.

Increased pro-inflammatory gene induction in *S. typhimurium*-infected *ptpn6* morphants is confirmed by RT-MLPA analysis

In addition to the microarray analysis, we used a recently described RT-MLPA assay that allows the simultaneous semi-quantitative PCR analysis of 34 innate immune genes (Rotman et al., 2011). Further confirming the microarray results, RT-MLPA analysis showed over 2-fold increased *S. typhimurium*-induced up-regulation in *ptpn6* morphants compared to controls for several cytokine/chemokine/interferon genes (*ccl-c5a*, *cxcl-c1c*, *ifnphi1*, *il1b*, *il8*, and *tnfa*), immune-related transcription factor genes (*fos*, *jun*, *junb*, *nfkb2*, and *rel*), the matrix metalloproteinase gene, *mmp9,* and the acidic chitinase gene, *chia.6* (Fig. 9). Additionally, five other genes that did not meet the significance thresholds in the microarray analysis (*ccl20*, *ccl-c24i*, *cxc46*, *fkbp5*, *tlr5a*) also showed over 2-fold higher up-regulation in *ptpn6* morphants based on RT-MLPA (Fig. 9). Of note, in both microarray and RT-MLPA analysis, the anti-inflammatory *il10* gene showed equal induction levels during *S. typhimurium* infection of *ptpn6* morphants and controls (Fig. 9, Supplementary Table 1). Based on the increased pro-inflammatory gene induction profile of *S. typhimurium*-infected *ptpn6* morphants, observed in microarray analysis and RT-MLPA, we conclude that *ptpn6* functions as a negative regulator of the innate immune response upon infection.

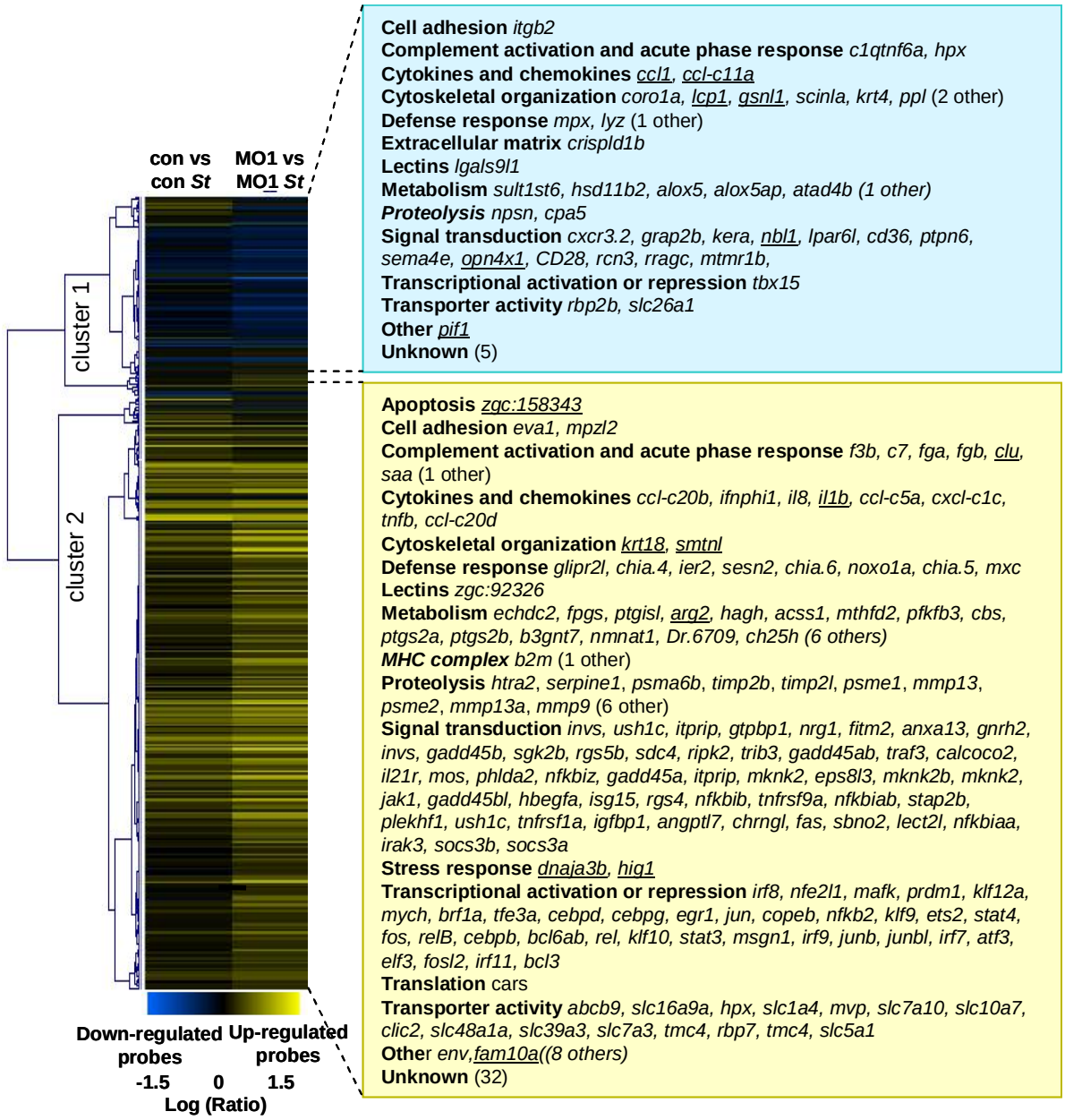

Figure 8. Gene groups showing higher up-regulation or stronger down-regulation upon *S. typhimurium* challenge of *ptpn6* morphants compared with *S. typhimurium* challenge of control embryos. A two-dimensional hierarchical clustering (average link, cosine correlation) was performed of the probes that were up-regulated or down-regulated by *S. typhimurium* infection in control embryos or in *ptpn6* morphants (fold change ≥1.5 and $P \leq 0.0001$). Up-regulated probes are indicated by increasingly brighter shades of yellow, and down-regulated probes are indicated by increasingly brighter shades of blue. Cluster 1 contains 78 probes (representing 51 different genes) that showed a stronger down-regulation in *S. typhimurium*-infected *ptpn6* morphants than *S. typhimurium*-infected control embryos, and cluster 2 contains 598 probes (representing 258 different genes) with stronger up-regulation in the *ptpn6* morphants. The gene symbols corresponding to the probes with stronger up- or down

regulation are indicated next to the two clusters, categorized in functional annotation groups. Only gene symbols of genes with assigned gene names are indicated in the figure, the number of other genes without a gene name in each annotation group is indicated between brackets; the full list is given in Supplementary Table 1. Symbols of genes that also showed differential expression in mock-injected *ptpn6* morphants compared to mock-injected control embryos are underlined.

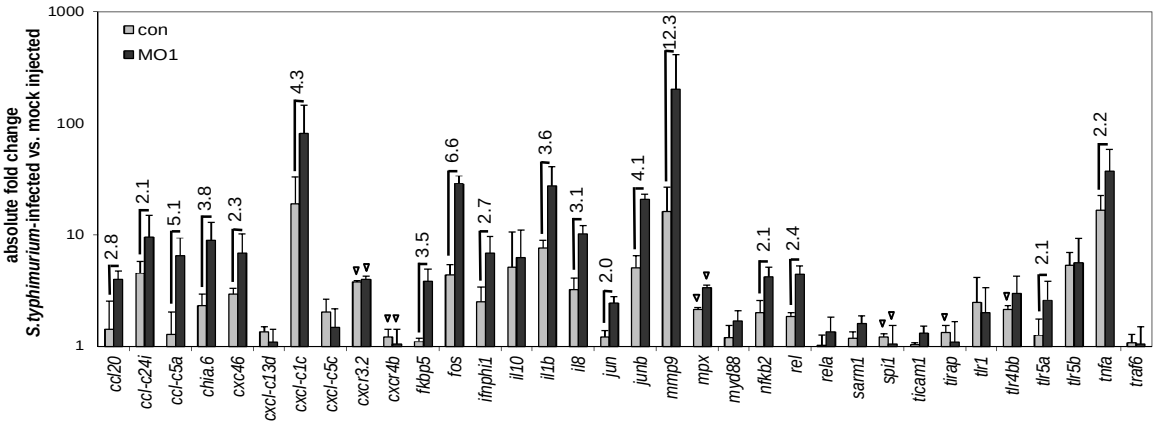

Figure 9. Hyperinduction of proinflammatory genes in *S. typhimurium*-infected ptpn6 morphants shown by RT-MLPA analysis. Relative expression levels of 34 innate immune response genes were determined as described in Rotman et al. 2011. The figure shows the absolute fold difference in expression of *S. typhimurium*-infected control embryos (con) and *ptpn6* morphants (MO1) versus the corresponding mock-injected groups. Data are plotted on a logarithmic scale. Values are the means ± standard deviation of three independent sample sets, which were the same as previously used for microarray analysis. Down-regulated expression is indicated with triangles. Numbers indicate ≥ 2-fold-change differences in up-regulated expression between *S. typhimurium*-infected *ptpn6* morphants and *S. typhimurium*-infected control embryos.

Discussion

The association of SHP1/PTPN6 deficiency with several types of chronic inflammatory disorders and with lymphoid and myeloid malignancies has raised substantial interest in this hematopoietic phosphatase as a drug target (Kundu et al., 2010). Here we exploited the zebrafish embryo as a novel animal model for studies on the function of the *ptpn6* gene. The late onset of adaptive immunity during zebrafish development permits studying *ptpn6* function in the sole context of innate immunity during embryo and larval development. Our results show that *ptpn6* deficiency in this model leads to pleiotropic defects at the late larval stage, accompanied by leukocyte infiltration and up-regulated inflammatory gene expression. Moreover, when embryos were challenged with bacteria during earlier stages of development, *ptpn6* knockdown enhanced the innate immune response to this infection. Despite this increased inflammatory response, *ptpn6*-deficient embryos were severely impaired in their ability to control infections, indicating the crucial importance of negative regulation by *ptpn6* for a balanced and functional innate immune response.

Inflammation-associated effects of *ptpn6* deficiency

Under normal culture conditions, without challenge by infection, *ptpn6* morphant larvae developed severe oedema and skin lesions by 5 to 6 days of age. The affected tissues in zebrafish *ptpn6* morphants were strongly infiltrated by leukocytes and increased numbers of TUNEL-positive apoptotic cells were also detected in these areas. Simultaneously, the overall expression levels of pro-inflammatory markers *il1b* and *mmp9* were over 10-fold increased. The observed inflammation in zebrafish *ptpn6* morphants is consistent with the function of mammalian SHP1 as a negative regulator of cytokine signaling, and is most likely caused by increased cytokine excretion by leukocytes which have been shown to exclusively express *ptpn6* (Zakrzewska et al., 2010). It remains unknown whether inflammation is the primary cause or the consequence of oedema and skin lesions in *ptpn6* morphants.

The observed phenotype is highly reminiscent of the severe skin inflammation observed in murine *Ptpn6* mutants, *me*, *mev,* and *spin* (Shultz et al., 1993; Tsui et al., 1993; Croker et al., 2008). In mice, *Ptpn6* deficiency, besides causing inflammation, was also associated with hyperproliferation of immune cells (Van Zant and Shultz, 1989), but we did not detect enhanced proliferation of myeloid cells during zebrafish embryonic and larval development. Among the three mutant alleles of *Ptpn6* in mice, *spin* causes the least severe functional knockdown (Croker et al., 2008). Inflammatory foot lesions of *spin* mutants did not develop when homozygotes were raised in a germ-free environment, showing the requirement of the normal microbiota to trigger this phenotype (Croker et al., 2008). However, *me* homozygotes born into a specific pathogen-free colony survived no better than under conventional conditions (Lutzner and Hansen, 1976). Similarly, we found that the late inflammation-associated phenotype of *ptpn6* morphant zebrafish larvae was equally severe when cultured using an established protocol to generate germ-free conditions (Pham et al., 2008). Complete germ-free conditions cannot be guaranteed during morpholino injections, but at least a major reduction of microbes was achieved in our experiments, since no bacterial colonies were observed when the culture medium of morpholino-injected larvae was plated on rich culture medium. Therefore, like in the *me* mutant, most likely another mechanism than the response to microbes is responsible for the development of spontaneous inflammation in *ptpn6* morphants.

In addition to the general inflammation-associated defects in *ptpn6* morphants, the dorsal area of the brain contained increased numbers of apoptotic cells as well as increased numbers of cells positive for the proliferation marker phosphohistone H3. Deregulation of pathways such as MAPK and NF-κB signaling, known to be affected by mammalian SHP1, may explain enhanced proliferation and apoptotic cell numbers in *ptpn6* morphants. The expression of *ptpn6* in wild type embryos and larvae by whole mount *in situ* hybridization was only detectable in myeloid cells and in the larval thymus (Zakrzewska et al., 2010). However, it cannot be excluded that *ptpn6* is also expressed in other tissues at lower levels, which may explain the specific hyperproliferative area in the brain of *ptpn6* morphants. In rodents, *Ptpn6* expression is

also predominantly hematopoietic, but has been detected in other tissues as well, including the CNS (Massa et al., 2000; Horvat et al., 2001).

Treatment with glucocorticoids enhanced the inflammatory phenotype, which is surprising since glucocorticoids are well known for their anti-inflammatory effects. They are widely used clinically to treat a variety of human immune-related diseases (Barnes, 2006) and their immune-suppressive effects appear to be well conserved between mammals and fish (Schaaf et al., 2009). Most anti-inflammatory effects of glucocorticoids are a result of the inhibitory interaction between the glucocorticoid receptor (GR) and transcription factors like AP-1 and NF-κB which are important for the up-regulation of many pro-inflammatory genes (De Bosscher and Haegeman, 2009). However, interaction with other transcription factors can enhance the activity of these proteins, and this may even lead to specific pro-inflammatory effects of glucocorticoids. In particular, interactions between GR and members of the STAT family, like STAT3, -5, and -6 have been demonstrated to be synergistic in nature (Zhang et al., 1997; Biola et al., 2000; Hermoso et al., 2004; Stoecklin et al., 1997; Rogatsky and Ivashkiv, 2006; Engblom et al., 2007). Interestingly, the JAK/STAT signaling pathway has been shown to be negatively regulated by SHP1 in many studies (Valentino and Pierre, 2006). Thus, the enhancement of the inflammatory phenotype upon *ptpn6* knockdown in zebrafish by glucocorticoids might be explained by a synergistic interaction between the GR and transcription factors, like the members of the STAT family, that have become activated due to the Ptpn6 deficiency (Fig. 10). Since in humans SHP1/PTPN6 deficiency has been shown to be possibly involved in the pathogenesis of several immune-related diseases, care should be taken when patients suffering from these diseases are treated with glucocorticoids. The SHP1 deficiency could be the cause of resistance to glucocorticoid treatment that is observed in a significant subpopulation of patients (Barnes and Adcock, 2009) and could theoretically even underlie a worsening of the disease state in response to this therapy.

Function of *ptpn6* in the response to bacterial infections

Knockdown of *ptpn6* impaired the ability of zebrafish embryos to control the proliferation of two bacterial pathogens that induce very different disease pathologies in the zebrafish embryo model: *S. typhimurium*, which causes acute disease, and *M. marinum*, which causes a chronic disease where bacteria persist in granulomatous aggregates. Even the growth of a normally non-pathogenic strain (*S. typhimurium* LPS O-Ag Ra mutant) could not be efficiently controlled and caused lethality. In contrast, murine *spin* mutants displayed increased resistance to *Listeria monocytogenes* (Croker et al., 2008). As discussed above, the *spin* phenotype is ascribed to a hypomorphic allele of *Ptpn6*, which may explain why this mutant is immunocompetent while zebrafish *ptpn6* morphants are not. The immunodeficiency of *ptpn6* morphants was apparent at early developmental stages well before the spontaneous increase in basal levels of pro-inflammatory genes and developmental defects that occur later during larval development. We found that the expression levels of immune-related transcription factor genes and many effector genes of the innate immune response were

hyperinduced upon infection in *ptpn6* morphants. In agreement, the whole set of hyperinduced genes showed significant enrichment of KEGG pathways related to pathogen recognition and cytokine signaling. These results support the function of *ptpn6* as a negative regulator of the innate immune response to bacterial infection. Since *ptpn6* morphants displayed decreased resistance, the hyperactivation of their innate immune response is apparently contra-productive for the organism's defense against bacterial pathogens.

The hyperinduction of innate immune response genes upon infection of *ptpn6* morphants was specific, since for example the expression levels of several myeloid markers were unchanged or reduced. In addition to many pro-inflammatory cytokines and transcription activators of the immune response, we also observed hyperinduction of other negative regulators than *ptpn6* itself. Apparently, in the absence of *ptpn6*, increased induction of other negative regulators was insufficient to prevent excessive inflammation and a contra-productive defense response against bacterial pathogens. This may be explained by the presumed inhibitory effect of Ptpn6 on many cytokine and immuno-receptors as well as central kinases in innate immunity signaling pathways (Abu-Dayyeh et al., 2008; Abu-Dayyeh et al., 2010), (Fig. 10). Furthermore, the anti-inflammatory cytokine gene *il10* was not induced to higher levels in infected *ptpn6* morphants than in controls. The fact that increased production of pro-inflammatory cytokines is not counteracted in *ptpn6* morphants by increased anti-inflammatory IL10 production is a possible explanation for their non-functional immune response against bacterial pathogens.

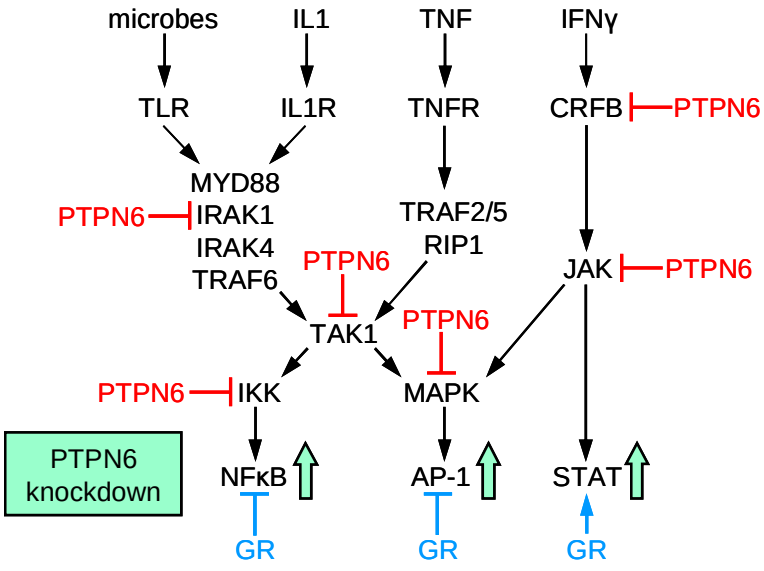

Figure 10. Model of PTPN6/SHP1 function in innate immunity signaling and interaction with glucocorticoid signaling. PTPN6/SHP1 has been proposed to inhibit cytokine receptors (like the CRFB family) as well as several kinases in TLR and cytokine signaling pathways (Abu-Dayyeh et al., 2008, Abu-Dayyeh et al., 2010). The putative inhibition motifs in these proteins are evolutionary conserved (Supplementary Table 2). Under conditions of PTPN6 deficiency the activation of transcriptional regulations like NFκB, AP-1 and STATs is enhanced (green arrows). Upon stimulation with glucocorticoids, the GR inhibits NF κB and AP-1 activity, but may have a synergistic interaction with STATs.

Interestingly, virulence factors of *Leishmania* parasites have been proposed to block macrophage functions by activation of SHP1 (Abu-Dayyeh et al., 2008; Gomez et al., 2009). Similarly, SHP1 activation by lipoarabinomannan (ManLAM) has been suggested as a host evasion strategy of *Mycobacterium tuberculosis* (Knutson et al., 1998; Rajos et al., 2002). Our results show the important regulatory function of this phosphatase in the host innate immune response to bacterial pathogens, which therefore could indeed be an attractive target for bacteria to manipulate. In our study, deficiency of *ptpn6* favored growth of *S. typhimurium* and *M. marinum* despite an enhanced innate immune response to these pathogens. These results are in line with studies of zebrafish embryos defective in TNF signaling or eicosanoid biosynthesis, which indicated that the outcome of *M. marinum* infection is worsened either when the fish produce high levels of anti-inflammatory lipoxins inhibiting TNF production, or when the fish produce pro-inflammatory leukotrienes and excessive levels of TNF (Clay et al., 2008; Tobin et al., 2010; Tobin et al., 2012). We have shown that the role of *ptpn6* is crucial for tightly regulating the induction levels of many key players in the innate immune response, identified by our microarray analysis, and conclude that the loss of *ptpn6* function results in a non-functional immune response to *S. typhimurium* and *M. marinum* infections.

Acknowledgements

We thank Mark van Eekelen and Vincent Runtuwene for initial experiments with the *ptpn6* splice morpholino, Janneke Rotman (BaseClear B.V.) for help with RT-MLPA analysis, Gerda Lamers for assistance with microscopy, Ulrike Nehrdich and Davy de Witt for fish care, and Peter Schoonheim and other group members for sharing protocols and helpful discussions. We further thank Steven Renshaw (University of Sheffield) for the mpx:gfp line, Brant Weinstein (NICHD, Bethesda) for the fli:gfp line, Shlomo Melmed (Cedars-Sinai Medical Center, Los Angeles) for the *pomc:gfp/prl:rfp* line, Anna Huttenlocher (University of Wisconsin) for L-plastin Ab, and Astrid van der Sar (VU Medical Center, Amsterdam) for bacterial strains and plasmids.

Supplementary data

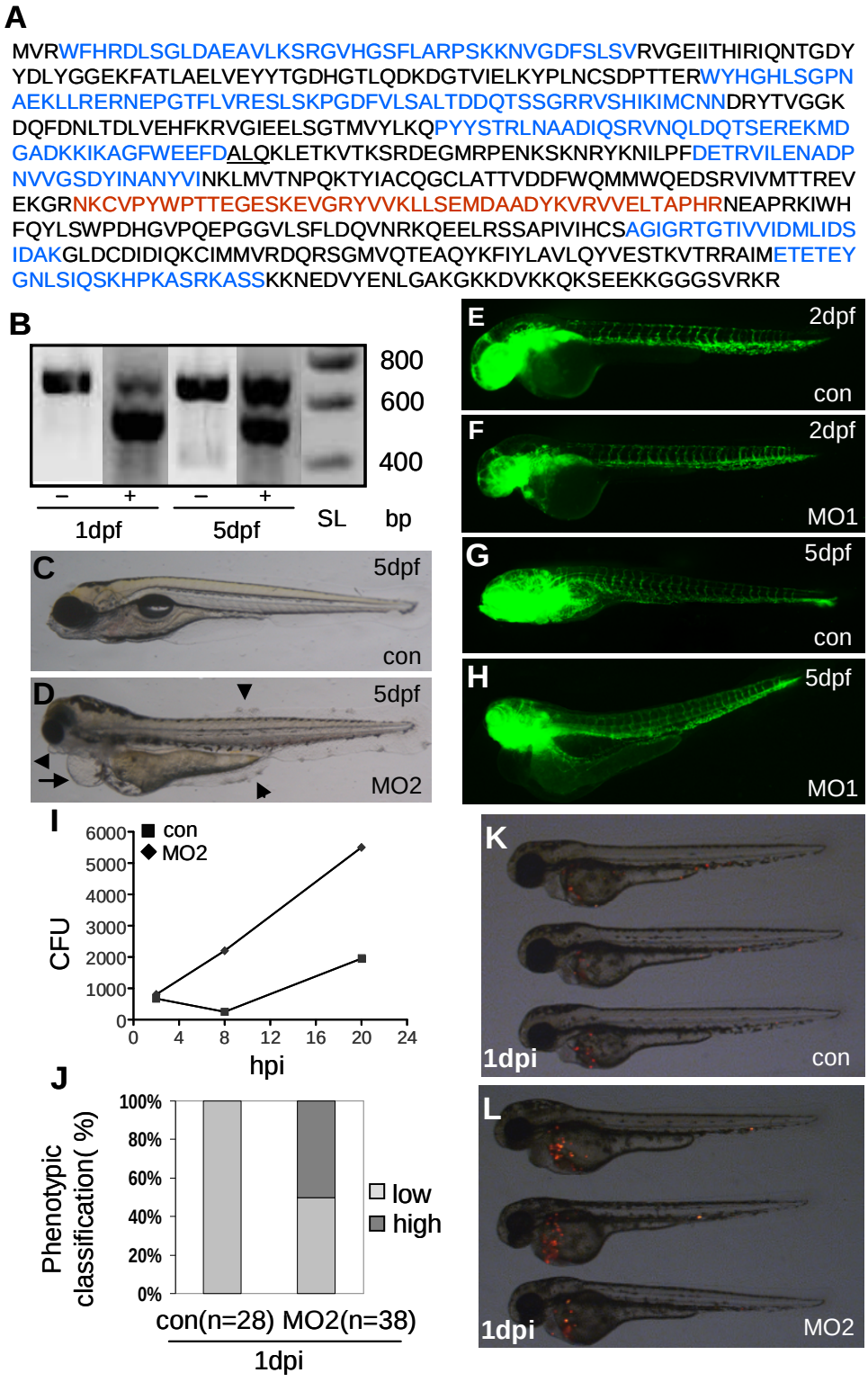

Supplementary Figure S1. Splice blocking morpholino effect and phenocopy with translation blocking morpholino. (A) The Ptpn6 protein sequence (Reference sequence NP_956254) is encoded by 16 exons. Amino acid sequences derived from different exons are indicated with alternating black and blue colours. The amino acid sequence deleted by injection of the splice blocking morpholino (MO1) is indicated in red. This sequence comprises the phosphatase catalytic domain. We note that the *ptpn6* genomic sequence on chromosome 16 in Ensembl Zv9 is erroneously split over two genes, ENSDARG00000089043, comprising coding exons 1-7, and ENSDARG00000013916, comprising coding exons 8-16. (B) Efficiency of the splice blocking morpholino. Embryos were injected at the 1-2 cell stage with Danieau's buffer (-) or with 1 nl of 0.06 mM *ptpn6* MO1 in Danieau's buffer (+) and RNA was isolated at 1 and 5 dpf. RT-PCR with forward primer in coding exon 8 (ATATTCAGAGCAGAGTAAATCAG) and reverse primer in exon 13 (TTCGTCACCTTCGTTTCC) results in a 698 bp product for the intact mRNA and a 563 bp product when exon 12 is skipped due to MO1 knockdown. MO1 knockdown of the intact mRNA is near complete at 1 dpf and partial at 5 dpf. SL, size ladder. (C) Phenotype of 5 dpf larva injected with standard control morpholino (con). (D). Phenotype of 5 dpf larva injected with translation blocking morpholino (MO2). In different experiments 5-10% of MO2-injected larvae showed cardiac oedema (arrow) and skin lesions (arrowheads) similar as observed with MO1 (Fig.1). (E-H) Fli1:EGFP embryos were injected with standard control mo (con, E,G) or *ptpn6* MO1 (F,H), Representative fluorescence images (lateral view, anterior to the left) were taken at 2 dpf (E, F) and 6 dpf (G, H). (I-L) Phenocopy of the *S. typhimurium* infection phenotype with a translation blocking morpholino (MO2). (I). Infection with *S. typhimurium* wild type strain. Embryos were injected with standard control morpholino (con) or *ptpn6* MO2 and infected with *S. typhimurium* at 28 hpf. Groups of 5 embryos were crushed in PBS at 2, 8, and 20 hpi, and dilutions were plated for CFU counting on LB medium with carbenicillin selection of the DsRED marker plasmid in *S. typhimurium*. A representative example of three independent experiments is shown. (J-L). Infection with *S. typhimurium* LPS mutant Ra strain. Embryos were injected with standard control morpholino (con) or *ptpn6* MO2 and infected with *S. typhimurium* Ra at 28 hpf. The bacterial burden was analyzed at 1 dpi based on fluorescence of the DsRED marker plasmid. A quantification of phenotypes (J) and stereo fluorescence images (lateral view, anterior to the left) of 3 embryos per group (K, L) are shown for a representative example of three independent experiments. The bacterial burden in embryos at 1 dpi was scored as low (representative image in K) or high (representative image in L).

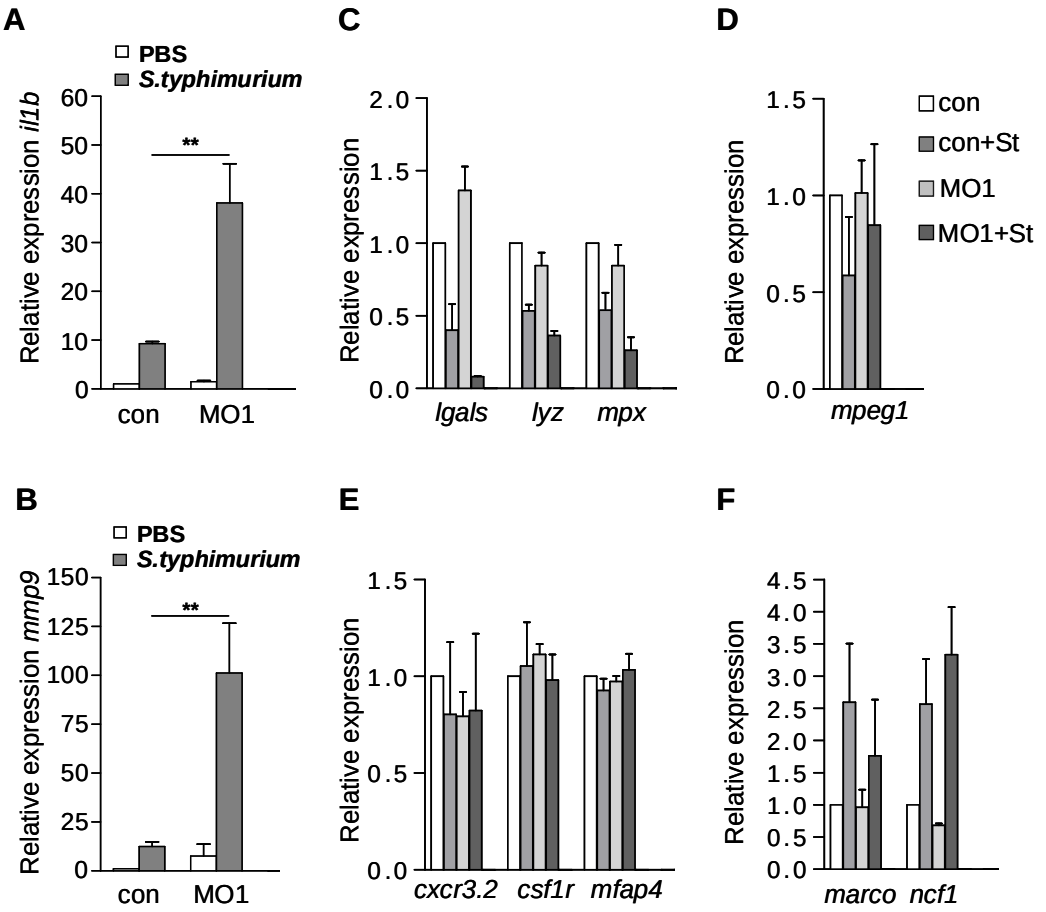

Supplementary Figure S2. qPCR analysis of *il1b*, *mmp9*, and leukocyte-specific genes in *ptpn6* morphants and control embryos infected with *S. typhimurium*. (A, B) Increased *ilb* (A) and *mmp9* (B) induction in infected *ptpn6* morphants compared to infected controls. (C-F) qPCR analysis of leukocyte-specific genes. qPCR analysis was performed on RNA samples from mock-injected (PBS) or *S. typhimurium*-infected (St) control embryos (con) and ptpn6 morphants (MO1). Relative expression levels are shown with the lowest expression level set at 1. Values are the means ± SEM of three independent sample sets, which were the same as previously used for microarray analysis. Asterisks in A and B indicate significant differences (**, P <0.01; **) tested by two-way ANOVA analysis with Bonferroni method as post-hoc test. Data for the leukocyte-specific genes were not significant by two-way ANOVA analysis and Bonferroni post-hoc test, but showed the same trend as the microarray data, i.e. stronger *S. typhimurium*-mediated down-regulation of *lgals9l1*, *lyz* and *mpx* show in *ptpn6* morphants than in controls (C), less pronounced *S. typhimurium*-mediated down-regulation of *mpeg1* in *ptpn6* morphants than in controls (D), unchanged expression of *cxcr3.2*, *csfr1*, and *mfap4* during *S. typhimurium* infection of *ptpn6* morphants and controls (E), and *S. typhimurium*-inducible expression of MARCO receptor homolog *LOC571584* and *ncf1* in both *ptpn6* morphants and controls (F).

Supplementary Table 1. microarray data of the *ptpn6* knockdown effect on the immune response to *Salmonella typhimurium* infection**.** Supplementary table can be found online at: https://www.dropbox.com/s/t3gyu0euewldyyv/Chapter2.suppl.table1.xlsx

Supplementary Table 2. Putative SHP1 binding sites in immune-related kinases**.** Supplementary table can be found online at: https://www.dropbox.com/s/5hgn84e9apiymgp/Chapter2.suppl.table2.xlsx

References

Abu-Dayyeh, I., B. Ralph, L. Grayfer, M. Belosevic, B. Cousineau, and M. Olivier. 'Identification of Key Cytosolic Kinases Containing Evolutionarily Conserved Kinase Tyrosine-Based Inhibitory Motifs (Ktims)', *Dev Comp Immunol* Vol. 34, No. 5, 481-4, 2010.

Abu-Dayyeh, I., M. T. Shio, S. Sato, S. Akira, B. Cousineau, and M. Olivier. 'Leishmania-Induced Irak-1 Inactivation Is Mediated by Shp-1 Interacting with an Evolutionarily Conserved Ktim Motif', *PLoS Negl Trop Dis* Vol. 2, No. 12, e305, 2008.

An, H., J. Hou, J. Zhou, W. Zhao, H. Xu, Y. Zheng, Y. Yu, S. Liu, and X. Cao. 'Phosphatase Shp-1 Promotes Tlr- and Rig-I-Activated Production of Type I Interferon by Inhibiting the Kinase Irak1', *Nat Immunol* Vol. 9, No. 5, 542-50, 2008.

Barnes, P. J. 'Corticosteroids: The Drugs to Beat', *Eur J Pharmacol* Vol. 533, No. 1-3, 2-14, 2006.

Barnes, P. J., and I. M. Adcock. 'Glucocorticoid Resistance in Inflammatory Diseases', *Lancet* Vol. 373, No. 9678, 1905-17, 2009.

Beutler, B. 'Microbe Sensing, Positive Feedback Loops, and the Pathogenesis of Inflammatory Diseases', *Immunol Rev* Vol. 227, No. 1, 248-63, 2009.

Biola, A., K. Andreau, M. David, M. Sturm, M. Haake, J. Bertoglio, and M. Pallardy. 'The Glucocorticoid Receptor and Stat6 Physically and Functionally Interact in T-Lymphocytes', *FEBS Letters* Vol. 487, No. 2, 229-33, 2000.

Christophi, G. P., M. Panos, C. A. Hudson, R. L. Christophi, R. C. Gruber, A. T. Mersich, S. D. Blystone, B. Jubelt, and P. T. Massa. 'Macrophages of Multiple Sclerosis Patients Display Deficient Shp-1 Expression and Enhanced Inflammatory Phenotype', *Lab Invest* Vol. 89, No. 7, 742-59, 2009.

Clay, H., H. E. Volkman, and L. Ramakrishnan. 'Tumor Necrosis Factor Signaling Mediates Resistance to Mycobacteria by Inhibiting Bacterial Growth and Macrophage Death', *Immunity* Vol. 29, No. 2, 283-94, 2008.

Croker, B. A., B. R. Lawson, S. Rutschmann, M. Berger, C. Eidenschenk, A. L. Blasius, E. M. Moresco, S. Sovath, L. Cengia, L. D. Shultz, A. N. Theofilopoulos, S. Pettersson, and B. A. Beutler. 'Inflammation and Autoimmunity Caused by a Shp1 Mutation Depend on Il-1, Myd88, and a Microbial Trigger', *Proc Natl Acad Sci U S A* Vol. 105, No. 39, 15028-33, 2008.

Croker, B. A., R. S. Lewis, J. J. Babon, J. D. Mintern, D. E. Jenne, D. Metcalf, J. G. Zhang, L. H. Cengia, J. A. O'Donnell, and A. W. Roberts. 'Neutrophils Require Shp1 to Regulate Il-1beta Production and Prevent Inflammatory Skin Disease', *J Immunol* Vol. 186, No. 2, 1131-9, 2011.

Cui, C., E. L. Benard, Z. Kanwal, O. W. Stockhammer, M. van der Vaart, A. Zakrzewska, H. P. Spaink, and A. H. Meijer. 'Infectious Disease Modeling and Innate Immune Function in Zebrafish Embryos', *Methods Cell Biol* Vol. 105, 273-308, 2011.

d'Alencon, C. A., O. A. Pena, C. Wittmann, V. E. Gallardo, R. A. Jones, F. Loosli, U. Liebel, C. Grabher, and M. L. Allende. 'A High-Throughput Chemically Induced Inflammation Assay in Zebrafish', *BMC Biol* Vol. 8, 151, 2010.

Davis, J. M., H. Clay, J. L. Lewis, N. Ghori, P. Herbomel, and L. Ramakrishnan. 'Real-Time Visualization of Mycobacterium-Macrophage Interactions Leading to Initiation of Granuloma Formation in Zebrafish Embryos', *Immunity.* Vol. 17, No. 6, 693-702, 2002.

De Bosscher, K., and G. Haegeman. 'Minireview: Latest Perspectives on Antiinflammatory Actions of Glucocorticoids', *Mol Endocrinol* Vol. 23, No. 3, 281-91, 2009.

Drexler, S. K., and B. M. Foxwell. 'The Role of Toll-Like Receptors in Chronic Inflammation', *Int J Biochem Cell Biol* Vol. 42, No. 4, 506-18, 2010.

Dubois, M. J., S. Bergeron, H. J. Kim, L. Dombrowski, M. Perreault, B. Fournes, R. Faure, M. Olivier, N. Beauchemin, G. I. Shulman, K. A. Siminovitch, J. K. Kim, and A. Marette. 'The Shp-1

Protein Tyrosine Phosphatase Negatively Modulates Glucose Homeostasis', *Nat Med* Vol. 12, No. 5, 549-56, 2006.

Engblom, D., J. W. Kornfeld, L. Schwake, F. Tronche, A. Reimann, H. Beug, L. Hennighausen, R. Moriggl, and G. Schutz. 'Direct Glucocorticoid Receptor-Stat5 Interaction in Hepatocytes Controls Body Size and Maturation-Related Gene Expression', *Genes Dev* Vol. 21, No. 10, 1157-62, 2007.

Eriksen, K. W., A. Woetmann, L. Skov, T. Krejsgaard, L. F. Bovin, M. L. Hansen, K. Gronbaek, N. Billestrup, M. H. Nissen, C. Geisler, M. A. Wasik, and N. Odum. 'Deficient Socs3 and Shp-1 Expression in Psoriatic T Cells', *J Invest Dermatol* Vol. 130, No. 6, 1590-7, 2010.

Geraldes, P., J. Hiraoka-Yamamoto, M. Matsumoto, A. Clermont, M. Leitges, A. Marette, L. P. Aiello, T. S. Kern, and G. L. King. 'Activation of Pkc-Delta and Shp-1 by Hyperglycemia Causes Vascular Cell Apoptosis and Diabetic Retinopathy', *Nat Med* Vol. 15, No. 11, 1298-306, 2009.

Gomez, M. A., I. Contreras, M. Halle, M. L. Tremblay, R. W. McMaster, and M. Olivier. 'Leishmania Gp63 Alters Host Signaling through Cleavage-Activated Protein Tyrosine Phosphatases', *Sci Signal* Vol. 2, No. 90, ra58, 2009.

Hermoso, M. A., T. Matsuguchi, K. Smoak, and J. A. Cidlowski. 'Glucocorticoids and Tumor Necrosis Factor Alpha Cooperatively Regulate Toll-Like Receptor 2 Gene Expression', *Mol Cell Biol* Vol. 24, No. 11, 4743-56, 2004.

Horvat, A., F. Schwaiger, G. Hager, F. Brocker, R. Streif, P. Knyazev, A. Ullrich, and G. W. Kreutzberg. 'A Novel Role for Protein Tyrosine Phosphatase Shp1 in Controlling Glial Activation in the Normal and Injured Nervous System', *J Neurosci* Vol. 21, No. 3, 865-74, 2001.

Huang da, W., B. T. Sherman, and R. A. Lempicki. 'Systematic and Integrative Analysis of Large Gene Lists Using David Bioinformatics Resources', *Nature protocols* Vol. 4, No. 1, 44-57, 2009.

Jopling, C., D. van Geemen, and J. den Hertog. 'Shp2 Knockdown and Noonan/Leopard Mutant Shp2-Induced Gastrulation Defects', *PLoS Genet* Vol. 3, No. 12, e225, 2007.

Knutson, K. L., Z. Hmama, P. Herrera-Velit, R. Rochford, and N. E. Reiner. 'Lipoarabinomannan of Mycobacterium Tuberculosis Promotes Protein Tyrosine Dephosphorylation and Inhibition of Mitogen-Activated Protein Kinase in Human Mononuclear Phagocytes. Role of the Src Homology 2 Containing Tyrosine Phosphatase 1', *J Biol Chem* Vol. 273, No. 1, 645-52, 1998.

Kozlowski, M., I. Mlinaric-Rascan, G. S. Feng, R. Shen, T. Pawson, and K. A. Siminovitch. 'Expression and Catalytic Activity of the Tyrosine Phosphatase Ptp1c Is Severely Impaired in Motheaten and Viable Motheaten Mice', *J Exp Med* Vol. 178, No. 6, 2157-63, 1993.

Kundu, S., K. Fan, M. Cao, D. J. Lindner, Z. J. Zhao, E. Borden, and T. Yi. 'Novel Shp-1 Inhibitors Tyrosine Phosphatase Inhibitor-1 and Analogs with Preclinical Anti-Tumor Activities as Tolerated Oral Agents', *J Immunol* Vol. 184, No. 11, 6529-36, 2010.

Lam, S. H., H. L. Chua, Z. Gong, T. J. Lam, and Y. M. Sin. 'Development and Maturation of the Immune System in Zebrafish, Danio Rerio: A Gene Expression Profiling, in Situ Hybridization and Immunological Study', *Dev.Comp Immunol.* Vol. 28, No. 1, 9-28, 2004.

Lawson, N. D., and B. M. Weinstein. 'In Vivo Imaging of Embryonic Vascular Development Using Transgenic Zebrafish', *Dev.Biol.* Vol. 248, No. 2, 307-318, 2002.

Lieschke, G. J., and N. S. Trede. 'Fish Immunology', *Curr Biol* Vol. 19, No. 16, R678-82, 2009.

Liu, N. A., Q. Liu, K. Wawrowsky, Z. Yang, S. Lin, and S. Melmed. 'Prolactin Receptor Signaling Mediates the Osmotic Response of Embryonic Zebrafish Lactotrophs', *Mol Endocrinol* Vol. 20, No. 4, 871-80, 2006.

Lutzner, M. A., and C. T. Hansen. 'Motheater: An Immunodeficient Mouse with Markedly Less Ability to Survive That the Nude Mouse in a Germfree Environment', *J Immunol* Vol. 116, No. 5, 1496-7, 1976.

Martin, J. S., and S. A. Renshaw. 'Using in Vivo Zebrafish Models to Understand the Biochemical Basis of Neutrophilic Respiratory Disease', *Biochem Soc Trans* Vol. 37, No. Pt 4, 830-7, 2009.

Massa, P. T., S. Saha, C. Wu, and K. W. Jarosinski. 'Expression and Function of the Protein Tyrosine Phosphatase Shp-1 in Oligodendrocytes', *Glia* Vol. 29, No. 4, 376-85, 2000.

Mathias, J. R., M. E. Dodd, K. B. Walters, J. Rhodes, J. P. Kanki, A. T. Look, and A. Huttenlocher. 'Live Imaging of Chronic Inflammation Caused by Mutation of Zebrafish Hai1', *J.Cell Sci.* Vol. 120, No. Pt 19, 3372-3383, 2007.

Meijer, A. H., and H. P. Spaink. 'Host-Pathogen Interactions Made Transparent with the Zebrafish Model', *Curr Drug Targets* Vol. 12, No. 7, 1000-17, 2011.

O'Neill, L. A. 'When Signaling Pathways Collide: Positive and Negative Regulation of Toll-Like Receptor Signal Transduction', *Immunity* Vol. 29, No. 1, 12-20, 2008.

Ordas, A., Z. Hegedus, C. V. Henkel, O. W. Stockhammer, D. Butler, H. J. Jansen, P. Racz, M. Mink, H. P. Spaink, and A. H. Meijer. 'Deep Sequencing of the Innate Immune Transcriptomic Response of Zebrafish Embryos to Salmonella Infection', *Fish Shellfish Immunol* Vol. 31, No. 5, 716-24, 2011.

Pao, L. I., K. Badour, K. A. Siminovitch, and B. G. Neel. 'Nonreceptor Protein-Tyrosine Phosphatases in Immune Cell Signaling', *Annual Review of Immunology* Vol. 25, 473-523, 2007.

Pham, L. N., M. Kanther, I. Semova, and J. F. Rawls. 'Methods for Generating and Colonizing Gnotobiotic Zebrafish', *Nat Protoc* Vol. 3, No. 12, 1862-75, 2008.

Renshaw, S. A., C. A. Loynes, D. M. Trushell, S. Elworthy, P. W. Ingham, and M. K. Whyte. 'A Transgenic Zebrafish Model of Neutrophilic Inflammation', *Blood* Vol. 108, No. 13, 3976-3978, 2006.

Rogatsky, I., and L. B. Ivashkiv. 'Glucocorticoid Modulation of Cytokine Signaling', *Tissue Antigens* Vol. 68, No. 1, 1-12, 2006.

Rojas, M., M. Olivier, and L. F. Garcia. 'Activation of Jak2/Stat1-Alpha-Dependent Signaling Events During Mycobacterium Tuberculosis-Induced Macrophage Apoptosis', *Cell Immunol* Vol. 217, No. 1-2, 58-66, 2002.

Rotman, J., W. van Gils, D. Butler, H. P. Spaink, and A. H. Meijer. 'Rapid Screening of Innate Immune Gene Expression in Zebrafish Using Reverse Transcription - Multiplex Ligation-Dependent Probe Amplification', *BMC Res Notes* Vol. 4, 196, 2011.

Schaaf, M. J., A. Chatzopoulou, and H. P. Spaink. 'The Zebrafish as a Model System for Glucocorticoid Receptor Research', *Comp Biochem Physiol A Mol Integr Physiol* Vol. 153, No. 1, 75-82, 2009.

Schoonheim, P. J., A. Chatzopoulou, and M. J. Schaaf. 'The Zebrafish as an in Vivo Model System for Glucocorticoid Resistance', *Steroids* Vol. 75, No. 12, 918-25, 2010.

Shultz, L. D., P. A. Schweitzer, T. V. Rajan, T. Yi, J. N. Ihle, R. J. Matthews, M. L. Thomas, and D. R. Beier. 'Mutations at the Murine Motheaten Locus Are within the Hematopoietic Cell Protein-Tyrosine Phosphatase (Hcph) Gene', *Cell* Vol. 73, No. 7, 1445-54, 1993.

Stockhammer, O. W., A. Zakrzewska, Z. Hegedus, H. P. Spaink, and A. H. Meijer. 'Transcriptome Profiling and Functional Analyses of the Zebrafish Embryonic Innate Immune Response to Salmonella Infection', *J Immunol* Vol. 182, No. 9, 5641-53, 2009.

Stoecklin, E., M. Wissler, R. Moriggl, and B. Groner. 'Specific DNA Binding of Stat5, but Not of Glucocorticoid Receptor, Is Required for Their Functional Cooperation in the Regulation of Gene Transcription', *Mol Cell Biol* Vol. 17, No. 11, 6708-16, 1997.

Stoop, E. J., T. Schipper, S. K. Huber, A. E. Nezhinsky, F. J. Verbeek, S. S. Gurcha, G. S. Besra, C. M. Vandenbroucke-Grauls, W. Bitter, and A. M. van der Sar. 'Zebrafish Embryo Screen for

Mycobacterial Genes Involved in the Initiation of Granuloma Formation Reveals a Newly Identified Esx-1 Component', *Dis Model Mech* Vol. 4, No. 4, 526-36, 2011.

Theofilopoulos, A. N., D. H. Kono, B. Beutler, and R. Baccala. 'Intracellular Nucleic Acid Sensors and Autoimmunity', *J Interferon Cytokine Res* Vol. 31, No. 12, 867-86, 2011.

Tobin, D. M., F. J. Roca, S. F. Oh, R. McFarland, T. W. Vickery, J. P. Ray, D. C. Ko, Y. Zou, N. D. Bang, T. T. Chau, J. C. Vary, T. R. Hawn, S. J. Dunstan, J. J. Farrar, G. E. Thwaites, M. C. King, C. N. Serhan, and L. Ramakrishnan. 'Host Genotype-Specific Therapies Can Optimize the Inflammatory Response to Mycobacterial Infections', *Cell* Vol. 148, No. 3, 434-46, 2012.

Tobin, D. M., J. C. Vary, Jr., J. P. Ray, G. S. Walsh, S. J. Dunstan, N. D. Bang, D. A. Hagge, S. Khadge, M. C. King, T. R. Hawn, C. B. Moens, and L. Ramakrishnan. 'The Lta4h Locus Modulates Susceptibility to Mycobacterial Infection in Zebrafish and Humans', *Cell* Vol. 140, No. 5, 717-30, 2010.

Tsui, F. W., A. Martin, J. Wang, and H. W. Tsui. 'Investigations into the Regulation and Function of the Sh2 Domain-Containing Protein-Tyrosine Phosphatase, Shp-1', *Immunol Res* Vol. 35, No. 1-2, 127-36, 2006.

Tsui, H. W., K. A. Siminovitch, L. de Souza, and F. W. Tsui. 'Motheaten and Viable Motheaten Mice Have Mutations in the Haematopoietic Cell Phosphatase Gene', *Nat Genet* Vol. 4, No. 2, 124-9, 1993.

Valentino, L., and J. Pierre. 'Jak/Stat Signal Transduction: Regulators and Implication in Hematological Malignancies', *Biochem Pharmacol* Vol. 71, No. 6, 713-21, 2006.

van der Sar, A. M., A. M. Abdallah, M. Sparrius, E. Reinders, C. M. Vandenbroucke-Grauls, and W. Bitter. 'Mycobacterium Marinum Strains Can Be Divided into Two Distinct Types Based on Genetic Diversity and Virulence', *Infect.Immun.* Vol. 72, No. 11, 6306-6312, 2004.

Van der Sar, A. M., R. J. P. Musters, F. J. M. Van Eeden, B. J. Appelmelk, C. M. J. E. Vandenbroucke-Grauls, and W. Bitter. 'Zebrafish Embryos as a Model Host for the Real Time Analysis of Salmonella Typhimurium Infections', *Cell.Microbiol.* Vol. in press 2003.

van der Sar, A. M., H. P. Spaink, A. Zakrzewska, W. Bitter, and A. H. Meijer. 'Specificity of the Zebrafish Host Transcriptome Response to Acute and Chronic Mycobacterial Infection and the Role of Innate and Adaptive Immune Components', *Mol Immunol* Vol. 46, No. 11-12, 2317-32, 2009.

van Eekelen, M., J. Overvoorde, C. van Rooijen, and J. den Hertog. 'Identification and Expression of the Family of Classical Protein-Tyrosine Phosphatases in Zebrafish', *PLoS One* Vol. 5, No. 9, e12573, 2010.

Van Zant, G., and L. Shultz. 'Hematologic Abnormalities of the Immunodeficient Mouse Mutant, Viable Motheaten (Mev)', *Exp Hematol* Vol. 17, No. 2, 81-7, 1989.

Witkiewicz, A., P. Raghunath, A. Wasik, J. M. Junkins-Hopkins, D. Jones, Q. Zhang, N. Odum, and M. A. Wasik. 'Loss of Shp-1 Tyrosine Phosphatase Expression Correlates with the Advanced Stages of Cutaneous T-Cell Lymphoma', *Hum Pathol* Vol. 38, No. 3, 462-7, 2007.

Wlodarski, P., Q. Zhang, X. Liu, M. Kasprzycka, M. Marzec, and M. A. Wasik. 'Pu.1 Activates Transcription of Shp-1 Gene in Hematopoietic Cells', *J Biol Chem* Vol. 282, No. 9, 6316-23, 2007.

Wu, C., M. Sun, L. Liu, and G. W. Zhou. 'The Function of the Protein Tyrosine Phosphatase Shp-1 in Cancer', *Gene* Vol. 306, 1-12, 2003.

Yu, C. C., H. W. Tsui, B. Y. Ngan, M. J. Shulman, G. E. Wu, and F. W. Tsui. 'B and T Cells Are Not Required for the Viable Motheaten Phenotype', *J Exp Med* Vol. 183, No. 2, 371-80, 1996.

Zakrzewska, A., C. Cui, O. W. Stockhammer, E. L. Benard, H. P. Spaink, and A. H. Meijer. 'Macrophage-Specific Gene Functions in Spi1-Directed Innate Immunity', *Blood* Vol. 116, No. 3, e1-11, 2010.

Zhang, J., A. K. Somani, and K. A. Siminovitch. 'Roles of the Shp-1 Tyrosine Phosphatase in the Negative Regulation of Cell Signalling', *Semin Immunol* Vol. 12, No. 4, 361-78, 2000.

Zhang, L., S. Y. Oh, X. Wu, M. H. Oh, F. Wu, J. T. Schroeder, C. M. Takemoto, T. Zheng, and Z. Zhu. 'Shp-1 Deficient Mast Cells Are Hyperresponsive to Stimulation and Critical in Initiating Allergic Inflammation in the Lung', *J Immunol* Vol. 184, No. 3, 1180-90, 2010.

Zhang, Z., S. Jones, J. S. Hagood, N. L. Fuentes, and G. M. Fuller. 'Stat3 Acts as a Co-Activator of Glucocorticoid Receptor Signaling', *The Journal of biological chemistry* Vol. 272, No. 49, 30607-10, 1997.

Zhu, Z., S. Y. Oh, Y. S. Cho, L. Zhang, Y. K. Kim, and T. Zheng. 'Tyrosine Phosphatase Shp-1 in Allergic and Anaphylactic Inflammation', *Immunol Res* Vol. 47, No. 1-3, 3-13, 2010.